Journal Pre-proof

Natural abundance sediment $\delta^{15}N$ as a proxy for long-term gross N-turnover processes, GHG emissions, and denitrification hotspots within fluvial ecosystems

Ricky Mwangada Mwanake , Elizabeth Gachibu Wangari , Hanna-Marie Kikowatz , Matti Allgaier , Allison Kolar , Ralf Kiese

PII: S2666-7657(26)00003-7
DOI: https://doi.org/10.1016/j.envadv.2026.100685
Reference: ENVADV 100685

To appear in: *Environmental Advances*

Received date: 10 October 2025
Revised date: 10 January 2026
Accepted date: 23 January 2026

Please cite this article as: Ricky Mwangada Mwanake , Elizabeth Gachibu Wangari , Hanna-Marie Kikowatz , Matti Allgaier , Allison Kolar , Ralf Kiese , Natural abundance sediment $\delta^{15}N$ as a proxy for long-term gross N-turnover processes, GHG emissions, and denitrification hotspots within fluvial ecosystems, *Environmental Advances* (2026), doi: https://doi.org/10.1016/j.envadv.2026.100685

Highlights

- Sediment $\delta^{15}N$ positively correlated with elevated fluvial GHG and N_2 saturation
- Sediment $\delta^{15}N$ enrichment occurred at N-rich streams with high N cycling rates
- Sediment $\delta^{15}N$ may indicate long-term hotspots of biogeochemical cycling in rivers

Title: Natural abundance sediment $\delta^{15}N$ as a proxy for long-term gross N-turnover processes, GHG emissions, and denitrification hotspots within fluvial ecosystems

Authors: [1]Ricky Mwangada Mwanake*, [1]Elizabeth Gachibu Wangari, [1]Hanna-Marie Kikowatz, [1]Matti Allgaier, [1]Allison Kolar, [1]Ralf Kiese

Corresponding author * email address: ricky.mwanake2@kit.edu

[1]Karlsruhe Institute of Technology, Institute for Meteorology and Climate Research, Atmospheric Environmental Research (IMK-IFU), Kreuzeckbahnstrasse 19, Garmisch-Partenkirchen 82467, Germany

Abstract

Nitrogen-rich agricultural headwater streams are known hotspots for fluvial greenhouse gas (GHG) emissions and denitrification, yet the underlying processes driving these elevated rates are not fully understood. In this study, we examined these mechanisms by combining measurements of gross nitrogen turnover processes, open-channel GHG and N_2 saturation (%) and fluxes, and $\delta^{15}N$ isotopic analysis of stream sediment and water at nine headwater stream sites with varying levels of agricultural land use. To assess seasonal patterns, data were collected across two transitional periods: spring–summer and winter–spring. Catchment land use emerged as an important environmental driver of variability, as open channel GHG emissions and denitrification rates were up to 11 times higher in fertilized grasslands and croplands compared to those in forested areas. In-vitro nitrogen turnover rates followed a similar trend and were mainly positively related to both GHG and N_2 oversaturation. This finding suggests that the excess nitrogen inputs in agricultural streams promote enhanced nitrogen turnover and gaseous carbon and nitrogen losses. We also observed a proportional increase in CO_2, CH_4, and N_2 saturation in the water column with sediment $\delta^{15}N$ enrichment, a known indicator of long-term nitrogen turnover processes. Because the highest GHG emissions and denitrification N_2 losses occurred within streams in fertilized areas, our findings highlight the potential of using sediment $\delta^{15}N$ as an indicator of long-term anthropogenic hotspots of fluvial GHG emissions and denitrification rates.

Keywords: Carbon dioxide, methane, nitrous oxide, headwater streams, gross nitrification rates, gross ammonification rates, isotopic pool dilution

1. Introduction

Streams and rivers are increasingly recognized as critical components of the global greenhouse gas (GHG) budget, contributing ~10 % of the global anthropogenic CO_2-equivalent emissions (Jones et al., 2023; Lauerwald et al., 2023b). In comparison to streams in natural landscapes, agricultural headwater streams in either fertilized grasslands or croplands are known hotspots of fluvial GHGs, with their GHG concentrations or emissions being several times higher than those observed in forested or other natural ecosystems (e.g., Borges et al., 2018; Mwanake et al., 2022; Mwanake et al., 2023a). While it is generally understood that the enhanced GHG production in agricultural streams is linked to excess nitrogen inputs from surrounding soils, the mechanistic understanding of the specific biogeochemical processes involved remains challenging to disentangle (Lauerwald et al., 2023a). This difficulty in source process understanding stems mainly from the general complexity of interconnected in-stream N cycling processes (e.g., Mulholland et al., 2009; Peterson et al., 2001; X. Xu et al., 2025), and the highly dynamic nature of N and dissolved GHG inputs from groundwater and surrounding landscapes (e.g., Liu et al., 2022; Mwanake et al., 2023b; Woodrow et al., 2024). Other factors that may also contribute to these complexities include the possible microbial community shifts with land use changes (e.g., Fasching et al., 2020) and the complex coupling of C and N cycling processes (e.g., Brookshire et al., 2005; Plont et al., 2020). For example, several studies have linked inputs of not only bioavailable nitrogen but also carbon in agricultural streams to land management practices such as fertilizer application, tillage, and plowing, which enhance soil erosion and mobilize organic matter (Arango & Tank, 2008; Drake et al., 2019; Graeber et al., 2015). Such bioavailable C and N additions can stimulate microbial GHG production processes such as nitrification and denitrification for N_2O, respiration for CO_2, and methanogenesis for CH_4 (Battin et al., 2023; Quick et al., 2019; Stanley et al., 2016).

In temperate regions, the timing and magnitude of bioavailable C and N inputs to streams are typically highly variable, often peaking during periods of fertilization or during hydrological events such as rainfall and snowmelt, which enhance terrestrial–aquatic connectivity (Ågren et al., 2010; Bellmore et al., 2018; Mwanake et al., 2023a). Additionally, light and temperature limitations during winter may constrain instream primary productivity, potentially altering the magnitude of N-driven biogeochemical processes (Arango & Tank, 2008; Kelly et al., 2021; Piña-Ochoa & Álvarez-Cobelas, 2006). These dynamics can lead to seasonal changes in fluvial GHG fluxes, driven partly by the temporal variability in biogeochemical process rates. Yet, process rate measurements that link enhanced nitrogen turnover processes to elevated GHG emissions in temperate riverine ecosystems across different seasons remain scarce (e.g., Beaulieu et al., 2011), with most studies relying on inferred relationships from their bivariate correlations with water quality parameters (Aho et al., 2021; Borges et al., 2018; Hu et al., 2016; Mwanake et al., 2023a).

Previous research on nitrogen cycling in streams has also primarily focused on process rates measured using laboratory-based sediment slurry assays that often employ nitrification or denitrification inhibitors (Arango & Tank, 2008; Kreiling et al., 2019; Speir et al., 2020; Vincent et al., 2025; X. Xu et al., 2025). While these approaches are relatively cheaper and offer valuable insights into instream nitrogen cycling, they face limitations, particularly regarding the uncertainty in scaling results to open-channel fluxes (Reisinger et al., 2016) and concerns about the effectiveness of the inhibitors themselves (Hall, 1984; Malone et al., 1998). In contrast, relatively few studies have employed open-channel techniques, such as isotopic tracer additions or direct field measurements of net rates, which are better suited to

capturing nitrogen cycling at the ecosystem scale (Mulholland et al., 2009; Mwanake et al., 2024; Peterson et al., 2001; Reisinger et al., 2016). In addition, most research on fluvial nitrogen cycling has primarily focused on nitrogen-limited forested ecosystems (e.g., Kemp & Dodds, 2002; Peterson et al., 2001; Piña-Ochoa & Álvarez-Cobelas, 2006), leaving significant gaps in our understanding of how anthropogenic nitrogen additions influence instream nitrogen cycling in both the short and the long term.

Natural abundance soil/sediment $\delta^{15}N$ isotopic signatures have shown great promise as integrative proxies for long-term nitrogen cycling processes in both terrestrial and aquatic ecosystems (Diebel & Zanden, 2009; Wangari et al., 2024; Liao et al., 2021; Peipoch et al., 2012). This is because the $\delta^{15}N$ isotopic signature of both soil/sediments reflects the cumulative effects of nitrogen inputs, transformations, and losses, including mineralization, nitrification, and denitrification, as well as shifts in nitrogen sources over extended timescales (Denk et al., 2017). Several studies in terrestrial ecosystems have linked enriched soil $\delta^{15}N$ values with increased anthropogenic nitrogen inputs and intensified nitrogen turnover rates (Craine et al., 2015; Wangari et al., 2024). Mechanistically, $\delta^{15}N$ values in the bulk soil/sediment become enriched or depleted as a result of isotopic fractionation through gradual nitrogen turnover processes over several years. When these turnover rates are high, more substantial isotopic fractionation occurs as the lighter isotope (^{14}N) is preferentially consumed during the microbial transformations, resulting in ^{15}N-depleted products and a progressive enrichment of ^{15}N in the residual substrate pool (Craine et al., 2015).

Because terrestrial and aquatic biogeochemical processes are tightly coupled through inter-ecosystem nutrient and sediment transfer, enriched sediment $\delta^{15}N$ values are also likely to indicate hotspots of nitrogen turnover rates within fluvial ecosystems. These hotspots may also be associated with nitrogen-driven increases in GHG emissions and denitrification N losses found in human-impacted streams (e.g., Beaulieu et al., 2011; Upadhyay et al., 2023). Despite its promise, the application of sediment $\delta^{15}N$ as a proxy for long-term nitrogen cycling and GHG emission potential in fluvial ecosystems remains underexplored, with so far only a few studies directly linking sediment isotopic composition to measured process rates or emission fluxes in aquatic ecosystems. (Marwick et al., 2014; Xia et al., 2022). To address key gaps in understanding the biogeochemical drivers of elevated GHG emissions and denitrification N losses in agricultural streams and their links to N cycling, this study aimed to: (1) quantify the spatial and temporal variability of nitrogen turnover process rates, GHG emissions, and open channel denitrification rates across a land use gradient (forest-grasslands-croplands) (2) measure stream sediments and water $\delta^{15}N$ isotopic values and assess their links with land use differences in instream nitrogen turnover processes, bioavailable forms of C and N, and oxygen depletion and 3) evaluate the potential of sediment $\delta^{15}N$ as a long-term proxy for identifying magnitude of GHG emission and N turnover processes at contrasting land uses.

2. Materials and methods

2.1 Site description

In this study, we sampled nine headwater stream sites (stream order 1-2) located within the southern Bavarian region of Germany (Figure 1; Table 1). The sites were selected primarily based on their dominant upstream land uses, with a focus on reference forest sites and fertilized agricultural sites that encompassed both grasslands and croplands. The rationale for choosing these three land uses/land covers was that they cumulatively account for almost two-thirds of the global land surface (Winkler et al., 2021), and also provide a gradient from natural to human-influenced ecosystems. Firstly, upstream catchment areas across the nine sites were delineated from a digital elevation model with a 30m resolution (Farr et al., 2007) using the "whitebox" package in R. The upstream land uses % of all the delineated catchments were then calculated from the Corine land cover 2018 survey (https://land.copernicus.eu/pan-european/corine-land-cover/clc2018?tab=mapview). Sites with greater than 50 % forest or agricultural (cropland + pasture) upstream land use were classified as either forested, grassland, or cropland streams, resulting in three forested, four grassland, and two cropland-dominated streams.

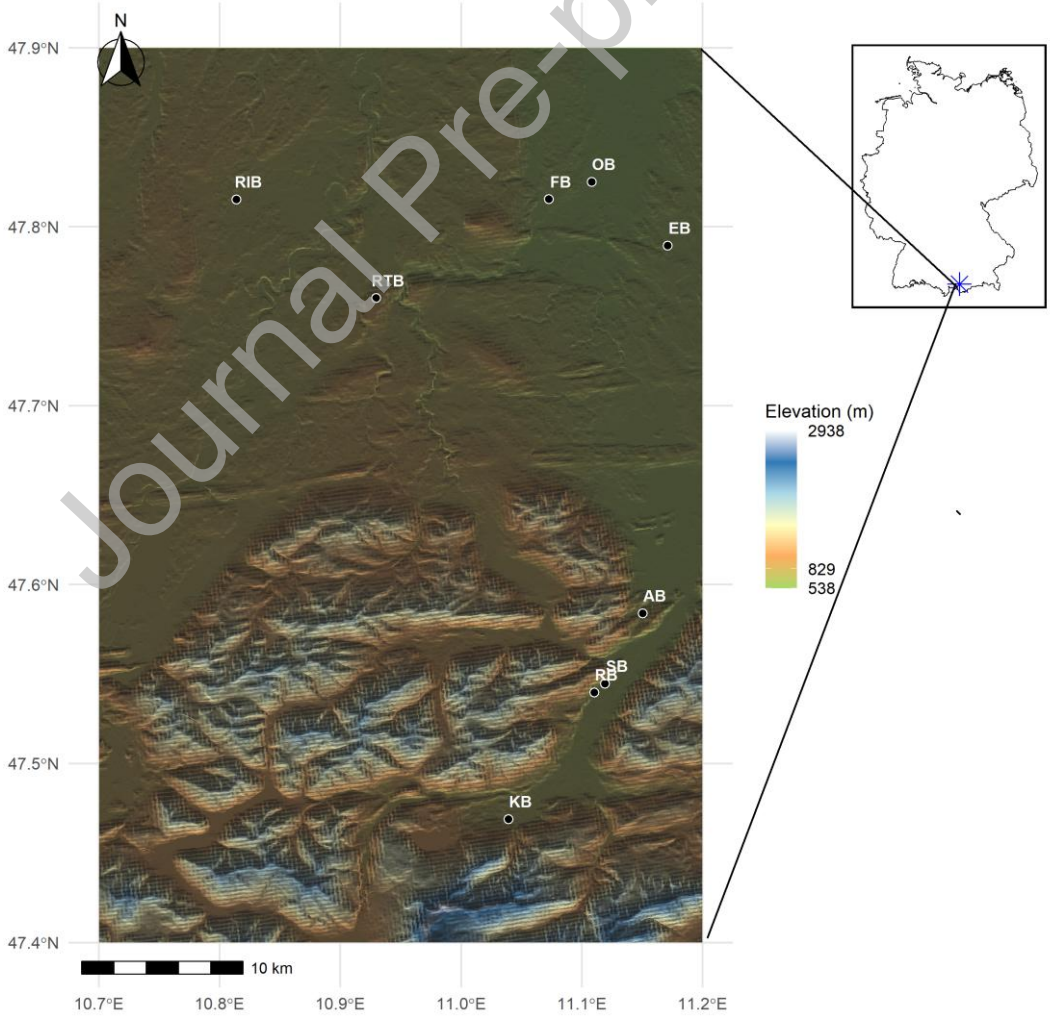

Figure 1: Location of the nine sampling sites within Germany (Table 1). The background map represents the elevation based on a STRM digital elevation model with a 30 m resolution (Farr et al., 2007).

Table 1: Summary descriptions of the nine sampled sites, including topographic and land use information

Site Name	Latitude	Longitude	Elevation	Stream length (m)	Stream slope (m m^{-1})	Land use (%)				
						Forest	Urban	Grassland	Cropland	Main Landuse
AB	47.584215	11.150458	725	940	0.150	100.0	0.0	0.0	0.0	Forest
EB	47.789396	11.171006	610	2085	0.005	17.0	1.1	29.0	51.9	Cropland
FB	47.815299	11.072626	598	2110	0.010	41.7	0.7	57.6	0.0	Grassland
KB	47.469052	11.039394	755	1254	0.020	83.6	1.1	15.2	0.0	Forest
OB	47.824306	11.109942	564	6188	0.054	31.1	9.1	53.0	6.9	Grassland
RB	47.540074	11.110434	664	1223	0.045	8.5	0.0	91.0	0.4	Grassland
RIB	47.815089	10.813883	738	1467	0.035	25.7	0.0	3.4	71.0	Cropland
RTB	47.758465	10.931351	894	654	0.037	99.5	0.0	0.5	0.0	Forest
SB	47.544055	11.119248	663	828	0.060	19.5	0.1	80.3	0.0	Grassland

2.2 Sampling strategy

Sampling was conducted across the nine sites in two five-week campaigns: the first during the spring-summer transition (May 7–June 11, 2024) and the second during the winter-spring transition (March 6–April 8, 2025). These transition periods were selected because they represented phases of increasing temperature with contrasting magnitudes. The spring-summer transition was hypothesized to capture warming from moderate to high temperatures, representing a substantial absolute increase in temperature that would enhance microbial metabolic rates. In contrast, sampling during the winter-spring transition captured warming from cold to moderate temperatures, a critical period for initiating biological activity following winter dormancy. Additionally, these periods were also hydrologically dynamic based on our past study in the region, characterized by snowmelt-driven discharge variability and precipitation pulses that influence gas exchange velocities, and the delivery of terrestrial dissolved gases, carbon, and nutrients fueling instream GHG evasion (See Mwanake et al., 2023a). Within each five-week campaign, weather conditions and in-stream discharge remained relatively stable, ensuring temporal consistency. The nine sites were also randomly sampled across the three dominant land uses to minimize potential confounding effects of short-term meteorological variability on the expected land-use-driven differences in instream biogeochemical processes.

2.3 Hydrological and water quality measurements

For each site visit, stream velocity was quantified using an electromagnetic sensor (OTT-MF-Pro, Hydromet, Germany). The stream slope was calculated from the STRM digital

elevation model with a 30 m resolution (Farr et al., 2007). In-situ water temperature (°C), pH, and dissolved oxygen (DO) (% saturation and mg L^{-1}) were quantified using the Pro DSS multiprobe (YSI Inc., USA). Water samples were collected for ammonium (NH_4-N), nitrate (NO_3-N), dissolved organic carbon (DOC), and total dissolved nitrogen (TN) analyses and filtered on-site using polyethersulfone (PES) filters that had been pre-leached with 20 mL of stream water. In the laboratory, these samples were analyzed for NH_4-N and NO_3-N concentrations using colorimetric methods, which involved measuring the absorbance of the samples with a microplate spectrophotometer (Model: Epoch, BioTek Inc., USA). The DOC and TN were measured using a TC/TN analyzer (DIMATOC, Dimatec, Germany). Dissolved organic nitrogen (DON) was calculated as the difference between TN and the two dissolved inorganic nitrogen (DIN) species.

2.4 Quantification of $\delta^{15}N$ in DIN

Using part of the water samples collected at each site, the natural abundance $\delta^{15}N$ in DIN was estimated by conducting successive chemical reduction and oxidation steps and then analyzing the isotopic signature from the final product N_2 (28, 29, 30) on a membrane inlet mass spectrometer (MIMS; Bay Instruments, USA). Firstly, NO_3-N in the samples was reduced to NH_4-N by zinc powder in an acidic medium. The liquid phase of the resultant mixtures was then gently transferred into the 12 mL vials until they were filled to the brim, and the vials were tightly capped with gas-tight septum caps. The next step involved oxidizing all the NH_4-N in the samples to dissolved N_2 (containing all three isotopes, with masses 28, 29, and 30) by adding 250 µL of oxidant solution (hypobromite iodine) through the gas-tight septum using a needle. The R_{29} in the sample (mass ratio 29:28) and standard (atmospheric nitrogen dissolved in water at 20 °C) were then analysed on the MIMS, and the $\delta^{15}N$-DIN (‰) in the sample was estimated according to equation 1.

$$\delta^{15}\mathrm{N} - \mathrm{DIN}\ (‰) = \left(\frac{R_{29}\ sample}{R_{29}\ standard} - 1\right) \times 1000 \qquad (1)$$

2.5 Open-channel CO_2, CH_4, and N_2O and N_2% saturation and flux measurements

As for the GHGs, CO_2, CH_4, and N_2O concentrations in the streams were measured by collecting in situ gas samples using the headspace equilibration technique, following published protocols (Aho & Raymond, 2019; Mwanake et al., 2022). Specifically, 80 ml of water was equilibrated with 20 ml of atmospheric air in a syringe after shaking for 2 minutes in the stream water to maintain in-situ temperatures. The headspace gas samples were transferred into 10 ml pre-evacuated glass vials for GHG concentration analysis in the laboratory using an SRI gas chromatograph (8610C, Germany) with an electron capture detector (ECD) for N_2O and a flame ionization detector (FID) with an upstream methanizer for simultaneous measurements of CH_4 and CO_2 concentrations. GHG concentrations were also quantified using a GC from air samples collected in 10 mL glass vials at each site (Table S1). GHG concentrations in the stream water (in moles L^{-1}) were then calculated using a mass balance approach as the sum of the post-equilibration gas concentrations in the headspace and water, after correcting for background GHG concentrations using the measured atmospheric air gas samples. For these calculations, the headspace gas concentrations were calculated using the Ideal Gas Law, while the water-phase gas concentrations were calculated using Henry's law (Aho & Raymond, 2019; Mwanake et al., 2022; Mwanake et al., 2025b).

Additional in-situ duplicate water samples were collected for N_2 concentration measurements by filling gas-tight 12 mL Exetainers underwater (Labco, UK) without air bubbles. The samples were then stored in a refrigerator at 2 °C until analysis. In the laboratory, measurements of dissolved N_2 (in moles L^{-1}) were carried out using the MIMS at near-in-situ temperatures, following the procedure outlined in Kana et al. (1994). We used

N_2:Ar current ratios to measure N_2 concentrations with high precision (<0.05 CV%) (Kana et al., 1994; An et al., 2001). The MIMS setup included a liquid N_2 trap and a reduction furnace to minimize water vapor and NO interference on the N_2 measurements (Kana et al., 1994). Both the GHG and N_2 concentrations were then expressed as % saturation (Equation 2). This calculation was performed by normalizing the actual concentrations in the water (C_{aq} in moles L^{-1}) to the stream water concentrations in equilibrium with site-scale measured atmospheric GHG concentrations and atmospheric pressure (C_{sat} in moles L^{-1}), based on Henry's gas solubility constants calculated at specific water temperatures.

$$GHG\ and\ N_2\ saturation\ (\%) = \left(\frac{C_{aq}}{C_{sat}}\right) \times 100 \qquad (2)$$

Open-channel diffusive fluxes (F) (mass m^{-2} d^{-1}) of the three GHGs and N_2 were then estimated using Fick's Law of gas diffusion, where the flux is the product of the gas exchange velocity (k) (m d^{-1}) and the difference between the stream water (C_{aq}) and the ambient atmospheric gas concentration in water, assuming equilibrium with the atmosphere (C_{sat}) (Equation 3).

$$F = k\ (C_{aq} - C_{sat}) \qquad (3)$$

The gas transfer velocities (k) for each of the gases were calculated from normalized gas transfer velocities (k_{600}) (m d^{-1}), modeled from measured site-scale stream velocity and slope values using equation 4 from Raymond et al. (2012), where V is stream velocity (m s^{-1}), and S is the slope (m m^{-1}).

$$k_{600} = VS^{0.76} \times 951.5 \qquad (4)$$

2.6 Quantification of in-vitro gross nitrification rates, gross ammonification rates, and net N_2 fluxes

We conducted sediment slurry incubations to measure process parameters. At each site, approximately 2 kg of fresh sediment was collected along a 5 m reach, homogenized, and filtered onsite to remove leaf litter, and then stored in acid-washed containers. Ten liters of bottom water were also collected for each site in acid-washed plastic containers. In the laboratory, the incubation experiment was divided into three parts: two for the gross rate measurements and one for the N_2 flux measurements. For the gross ammonification (GAR) and gross nitrification rates (GNR), 20 g of fresh sediment and 100 mL of stream water were initially added to 250 mL glass flasks (Sigma Aldrich) (16 flasks, with 8 designated for the GAR and 8 for the GNR). To one batch of 8, we added 2 mL of ^{15}N-KNO_3 (5000 µmoles-N L^{-1}, ^{15}N at 99%) for quantifying gross nitrification rates (GNR), and to the other batch of 8 bottles, we added 2 mL of ^{15}N-NH_4Cl (5000 µmoles-N L^{-1}, ^{15}N at 99%) for quantifying gross ammonification rates using the isotopic pool dilution method (Murphy et al., 2003). On average, the ^{15}N additions accounted for 12.7% of background extractable sediment NO_3-N concentrations and 34.8% of extractable sediment NH_4-N concentrations (Table S2). These enrichment levels ensured detectable ^{15}N dilution while remaining within the range commonly recommended to minimize stimulation of in situ nitrogen consumption processes (Murphy et al., 2003; 5-25 % of background levels). For the N_2 flux measurements, 40 g of fresh sediment and 210 mL of stream water were incubated in 8 additional flasks with no headspace.

The 8 bottles for the three analyses included 4 replicates for initial conditions before incubation (T_0) and 4 replicates to be sampled after incubation (T_1). After the setup, all 24 bottles were capped with gas-tight lids. The glass bottles were placed in the shaker at 250 rpm for mixing. After mixing on the shaker for 4 minutes, half of the bottles (12) were incubated in the dark for 42 hours in a shaking incubator (rpm 120, 20 °C). The other half was

destructively sampled to determine initial concentrations of total NH_4-N, ^{15}N-NH_4, total NO_3-N, ^{15}N-NO_3, and N_2 concentrations. The same destructive sampling method was applied to the 12 bottles after incubation. While the micro-scale redox conditions within the incubation bottles used to measure gross nitrification, gross ammonification, and N_2 fluxes may not have fully replicated in situ field conditions, our rationale for conducting experiments with a headspace (gross nitrification and ammonification) and without a headspace(N_2), combined with continuous shaking, was to represent turbulent riverine environments in which sediment, water, and air phases interact dynamically.

For DIN concentration measurements, destructive sampling involved transferring 10 mL of the sediment slurry to 50 mL centrifuge tubes and adding 40 mL of 1 M KCl to extract DIN. During extraction, the KCL and the slurry mixtures were shaken for 1 hour at 250 rpm. The mixtures were then allowed to decant, and the upper waters were filtered through a 0.45 μm pore-size PES filter for later analyses of total NH_4-N, ^{15}N-NH_4, total NO_3-N, ^{15}N-NO_3 concentrations in the filtrates. From the extracts, total NH_4-N and NO_3-N concentrations were analyzed using the colorimetric method described above. The ^{15}N-NH_4 and ^{15}N-NO_3 concentrations were analysed using the REOX/MIMS method on the MIMS (Lin et al., 2017, 2021). Measurements of initial and final dissolved N_2 were also carried out on the MIMS following the procedure outlined in Kana et al. (1994).

After quantifying the initial and final DIN concentrations, gross ammonification and gross nitrification rates were then calculated based on equation 4, where by the GR represent either GAR or GNR in μg N g^{-1} d^{-1}, M_i and M_f are the individual concentrations of total NH_4-N for GAR or total NO_3-N for GNR in the initial and final sediment-slurries in μg N g^{-1}, H_i and H_f are the respective concentrations of ^{15}N-NH_4 for GAR or ^{15}N-NO_3 for GNR in initial and final sediment in μg N $g^{-1,}$ and t is the incubation time in days (Equation 5; Murphy et al., 2003). Theoretically, the pool dilution method calculates the gross rate (GR) of a nitrogen transformation process by measuring how quickly a labeled tracer (in this case ^{15}N-NH_4 or ^{15}N-NO_3) is diluted within the substrate pool over time. The first term *Mi−Mf* represents the net fluxes of the total DIN species (or substrate) pool size over time. The logarithmic correction factor accounts for the dilution of the ^{15}N tracer by the unlabeled N produced, allowing the back-calculation of the actual gross rate from the observed changes in both pool size and the enriched tracer. When the first term (net fluxes) is multiplied by this correction factor, it yields the gross production rate of the process.

$$GR = \frac{M_i - M_f}{t} \times \frac{\log(\frac{H_i \times M_f}{H_f \times M_i})}{\log(\frac{M_i}{M_f})} \quad (5)$$

The net N_2 fluxes during the incubations were calculated using Equation 6, where FN_2 is the N_2 fluxes in μg g^{-1} d^{-1}, C_i and C_f are the respective concentrations of N_2 in initial and final sediment-slurries in μg g^{-1}, and t is the incubation time in days.

$$FN_2 = \frac{C_f - C_i}{t} \quad (6)$$

2.7 Sediment C content, N content, C:N ratio, and $\delta^{15}N$ measurements

About 0.5 kg of the remaining fresh sediment sample was oven-dried to a constant weight at 60 °C. Then, 50 g of the dry sediment was ball-milled into a fine powder for measurements of sediment C content, N content, C:N ratio, and $\delta^{15}N$ that were performed

simultaneously using an elemental analyzer (EA 1110, CE instrument) coupled in a continuous flow mode to an IRMS (DELTA^{PLUS}, Finnigan MAT: Precision = 0.15 ‰). The natural abundances of $\delta^{15}N$ in the sediment samples were expressed relative to those in the standard (Equation 7), where R_{sample} is the N ($^{15}N/^{14}N$) isotope ratio measured in the samples, and $R_{standard}$ is the isotope ratio in the standard (atmospheric N_2).

$$\delta^{15}N\ (‰) = \left(\frac{R_{sample}}{R_{standard}} - 1\right) \times 1000 \qquad (7)$$

2.8 Statistical analyses

We applied a non-parametric post-hoc Dunn's test to identify significant ($p < 0.05$) seasonal and land-use differences in water quality parameters, nitrogen cycling rates, and CO_2, CH_4, N_2O, and N_2 saturation and fluxes. In this non-parametric test, we employed the Benjamini–Hochberg (BH) method due to its ability to control the false discovery rate. To identify the key environmental and biogeochemical predictors of open channel CO_2, CH_4, N_2O, and N_2 oversaturation, we applied both bivariate regression models and multivariate regression models using the glmnet package in R. The bivariate models were used to examine linkages between sediment $\delta^{15}N$ enrichment and nitrogen cycling, GHG, and N_2 saturation hotspots. The multivariate models assessed how these relationships covary with other key water quality parameters.

Before model construction, all GHG and N_2 saturation values were transformed using the natural logarithm to meet the assumption of normality required for these models. The predictor variables in each of the multivariate models included dissolved organic carbon (DOC), dissolved organic nitrogen (DON), dissolved inorganic nitrogen (DIN), dissolved oxygen (DO) saturation (%), agricultural land use percentage, sediment $\delta^{15}N$ and in-vitro N turnover process rates (N_2 flux, gross ammonification rate (GAR), and gross nitrification rate (GNR). The rationale for choosing these variables was that they represented either substrates, indicators, or actual GHG production and consumption processes within streams (Battin et al., 2023; Mwanake et al., 2024; Stanley et al., 2016). All predictor variables were standardized (centered and scaled) prior to model fitting to ensure that coefficient estimates were directly comparable across variables with different units and scales. For the multivariate analysis, we used elastic net regression (with the alpha parameter set at 0.5), which combines L1 (LASSO) and L2 (ridge) penalties to perform variable selection and handle multicollinearity among predictors simultaneously. The optimal regularization parameter (λ) was then selected using a 5-fold cross-validation, with coefficients extracted at λ = lambda.1se to favor model interpretability and reduce overfitting. This approach shrinks coefficients of less influential predictors toward zero, effectively performing automated feature selection while retaining interpretability. Model performance was assessed using R^2, calculated as the proportion of variance explained by the selected predictors. All these analyses were conducted in R version 4.4.0.

3. Results

3.1 Spatial-temporal trends in water quality parameters

Across the two transitional sampling periods, from spring to summer and from winter to spring, in-stream DIN (ammonium (NH_4-N) and nitrate (NO_3-N)) and their $\delta^{15}N$ isotopic signatures exhibited the most substantial variability, ranging by up to 2 orders of magnitude (Table S3). In contrast, stream water pH had the least variation (Table S3). Water temperature and the $\delta^{15}N$-DIN showed significant seasonal patterns, with higher temperatures in the spring-summer period coinciding with up to 7‰ higher $\delta^{15}N$-DIN isotopic values across the three land uses (Figure 2).

However, land-use rather than seasonal differences accounted for most of the variability in water-quality parameters, following gradients from forest to grassland to cropland (Figure 2). For instance, DO saturation was significantly higher in forested streams than in grassland streams in the spring-summer transition, but showed no significant land use differences during the winter-spring transition. NH_4-N concentrations exhibited similar land-use patterns during the spring–summer period, with higher values in forested streams than in grassland and cropland streams (Figure S1; Table S4). NO_3-N and TN were up to 8.8 times higher in cropland streams compared to those in grasslands and forests, with the most pronounced differences observed during the winter–spring transition (Figure 2; Figure S1; Table S4). The high TN concentrations in cropland streams relative to DOC resulted in significantly lower DOC:TN ratios at these sites than in grassland and forested streams during both sampling periods (Figure 2; Figure S2).

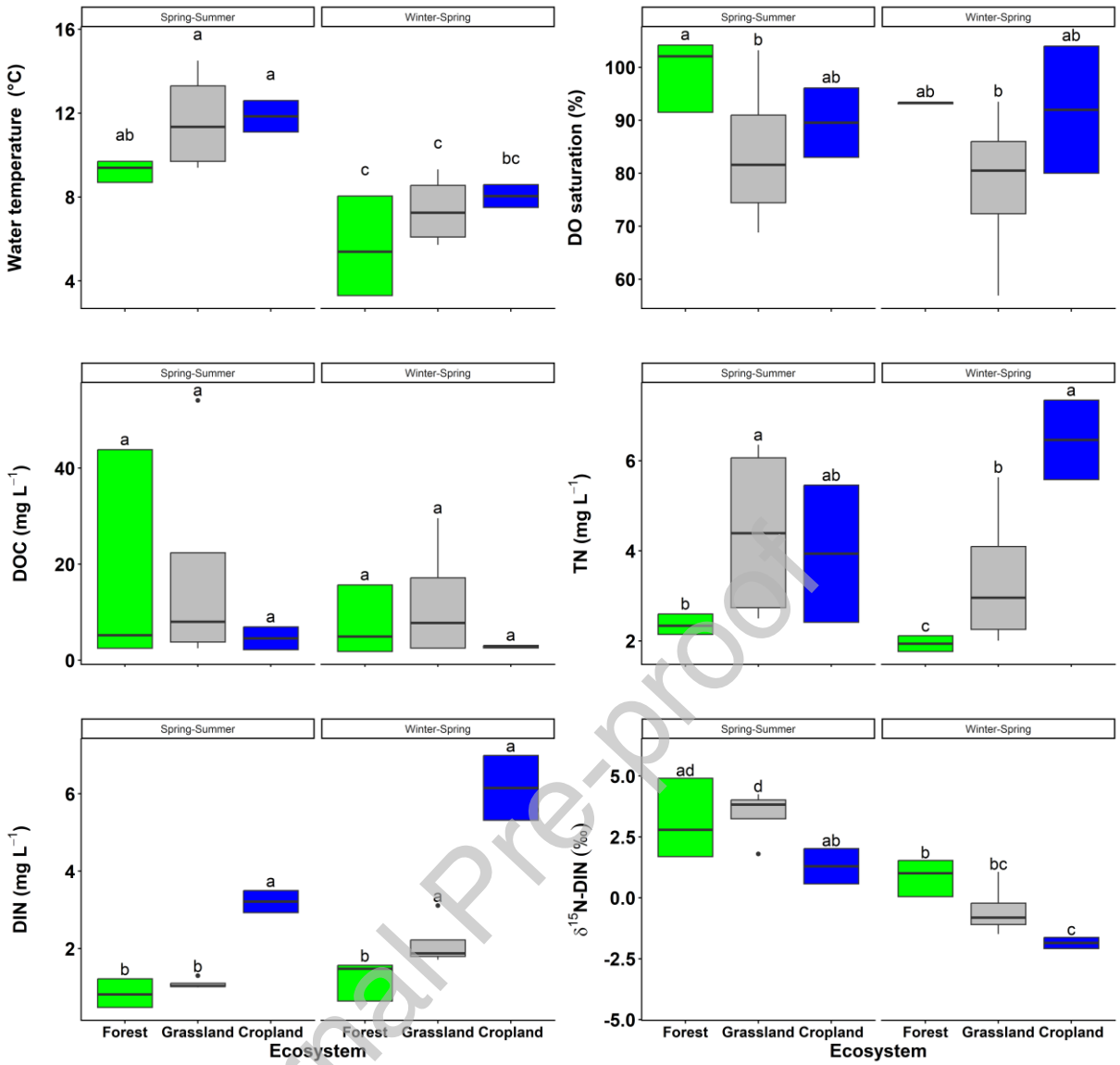

Figure 2: Seasonal and land use patterns of key water quality parameters across nine sites (forest=3, grassland = 4, cropland =2). Differences in the letters on top of the boxplots represent significant ($p < 0.05$) combined differences across seasons and land use, based on the non-parametric post-hoc Dunn's test.

Similar to NO_3-N, the total DIN pool showed consistent land-use patterns across seasons, with significantly higher concentrations in cropland streams than in grassland streams and forested streams (Figure 2). Opposite trends, however, were observed for the δ^{15}N-DIN isotopic values, which were significantly more enriched in forested and grassland streams than in cropland streams (Figure 2). These opposing trends resulted in a significant positive relationship between site-scale δ^{15}N-DIN isotopic values and the inverse of DIN concentration, with trends along the regression line driven by both seasonal and land-use differences (Figure S3). For example, we observed the most depleted δ^{15}N-DIN isotopic values at cropland sites, which had the highest DIN concentrations during the winter-spring period. In contrast, the most enriched δ^{15}N-DIN values appeared at a forested site during the spring-summer transition, which also had the lowest DIN concentration (Figure S3).

3.2 Spatial-temporal trends in in-vitro nitrification, ammonification, and denitrification rates

Similar to the water quality parameters, N cycling process rates exhibited high variability throughout the study period, with in-vitro gross nitrification rates (GNR) and denitrification (N_2) rates varying by up to two orders of magnitude (Table S3). Specifically, gross nitrification rates, gross ammonification (GAR) rates, and denitrification rates ranged from 0.02 – 3.15 $\mu g\ N\ g^{-1}\ d^{-1}$, 0 – 2.5 $\mu g\ N\ g^{-1}\ d^{-1}$, and 0.08 – 5.39 $\mu g\ N_2\ g^{-1}\ d^{-1}$, respectively. In contrast, net nitrification and net ammonification rates showed much narrower ranges, from -0.48 – 0.51 and -0.36 – 0.04 $\mu g\ N\ g^{-1}\ d^{-1}$, respectively. Mean gross N turnover rates were up to 8.8 times higher than net rates, but up to 1.8 times lower than denitrification rates (Table S3).

Like the water quality parameters, land use rather than seasonality was the primary driver of variability in the nitrogen cycling processes (Figure 3). For instance, GAR and GNR were up to 3.3 times higher in cropland streams compared to forested streams during the winter–spring period. GNR and denitrification rates also showed similar land use differences during the spring–summer period, though the GNR differences were not statistically significant (Table S4; Figure 3). However, cumulative nitrogen cycling processes consistently followed the same trend, with higher rates observed in cropland or grassland streams than in forested streams across both seasonal transitions (Figure 3). In contrast to gross rates, net ammonification and nitrification rates exhibited minimal to no significant variation across seasons or land uses (Figure S1).

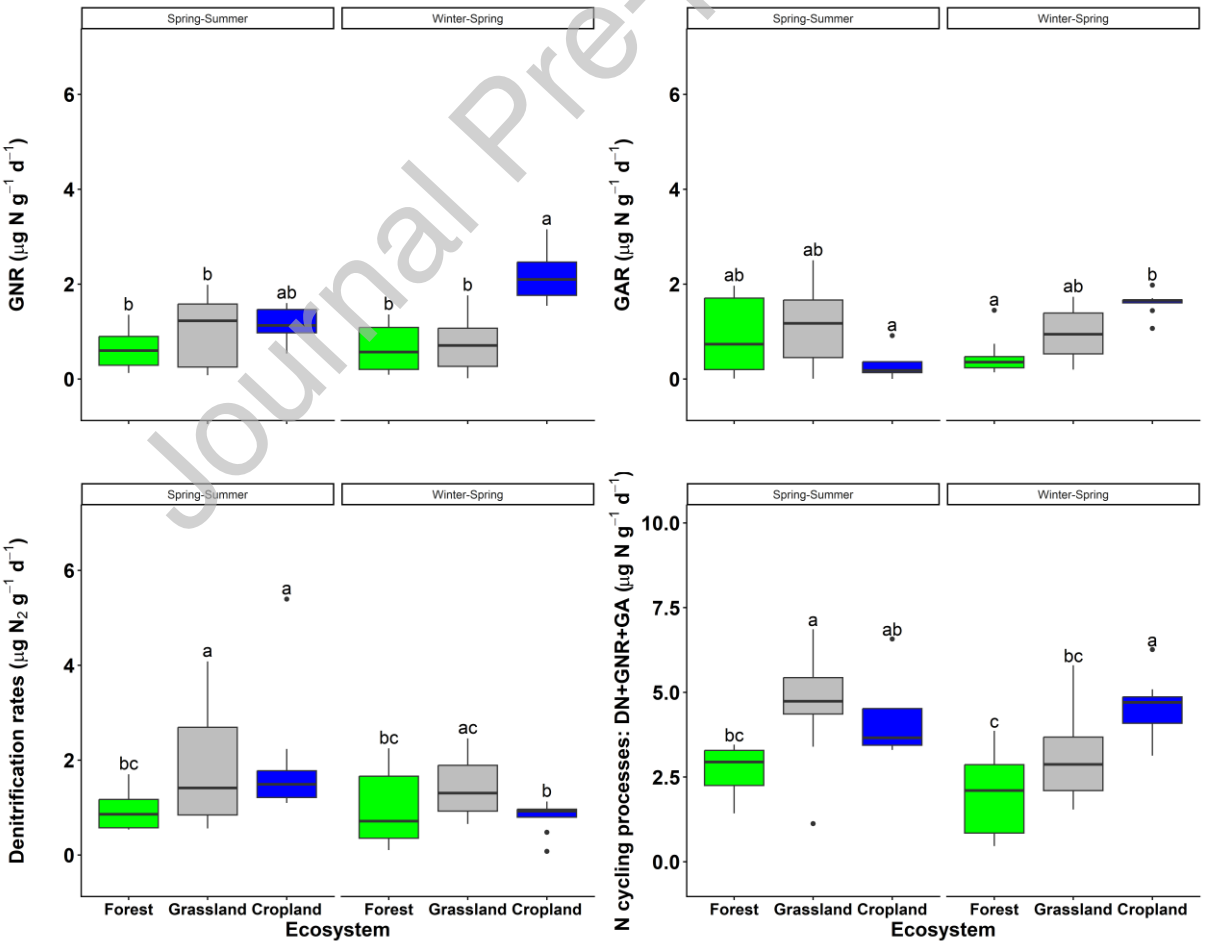

Figure 3: Seasonal and land use patterns of in-vitro gross nitrification rates (GNR), gross ammonification rates (GAR), denitrification rates (DN), and their combined rates across nine sites (forest=3, grassland = 4, cropland =2). Differences in the letters on top of the boxplots represent significant ($p < 0.05$) combined differences across seasons and land use, based on the non-parametric post-hoc Dunn's test.

3.3 Spatial-temporal trends in GHG emissions and open-channel denitrification (N_2 fluxes)

Stream greenhouse gas (GHG) concentrations were predominantly oversaturated relative to atmospheric equilibrium, with mean (± SE) saturation values of 646 ± 62% for CO_2, 2682 ± 455% for CH_4, and 160 ± 18% for N_2O (Table S3). GHG saturation levels also varied by up to three orders of magnitude, with the largest variability observed for CH_4, ranging from 49 – 14335%. In comparison, CO_2 and N_2O exhibited lower variability, ranging from 88 – 1873% and 51 – 689%, respectively (Table S3). Like GHGs, open-channel N_2 concentrations were also mostly oversaturated during the study period, ranging from 92.7–108.4% (mean: 101.7 ± 0.5%). Estimated fluxes ranged from -0.2 –66.5 g m^{-2} d^{-1} for CO_2-C (mean: 13.9 ± 2.1), -0.2 – 37.7 mg m^{-2} $d^{-1}$for CH_4-C (mean: 8.6 ± 1.4), -4.18 – 5.04 mg m^{-2} $d^{-1}$for N_2O-N (mean: 0.4 ± 0.3), and -15.8 – 35.0 g m^{-2} d^{-1} for N_2 (mean: 1.54 ± 1.7).

Similar to the patterns observed in water quality, nitrogen cycling processes, and sediment characteristics, variability in GHG and N_2 saturation and fluxes was mainly influenced by land use (Figure 4; Figure S4). Specifically, CO_2, N_2O, and N_2 saturation values were up to 4.9 times higher in cropland and grassland streams than in forested streams during the study period. In contrast, CH_4 saturation values, which differed among agricultural streams, were higher in grasslands than in both forested and cropland streams (Figure 4, Table S4). GHG and N_2 fluxes followed similar patterns to their saturation values, and were up to 11 times higher in the agricultural streams than in forested ones. Regarding seasonality, cropland and grassland streams exhibited the most substantial variability, generally showing higher CO_2 fluxes during the spring–summer transition, whereas N_2O showed the opposite trend, peaking during the winter–spring period. In contrast to these two GHG fluxes, seasonality had a limited overall influence on CH_4 and N_2 fluxes (Figure S4, Table S4).

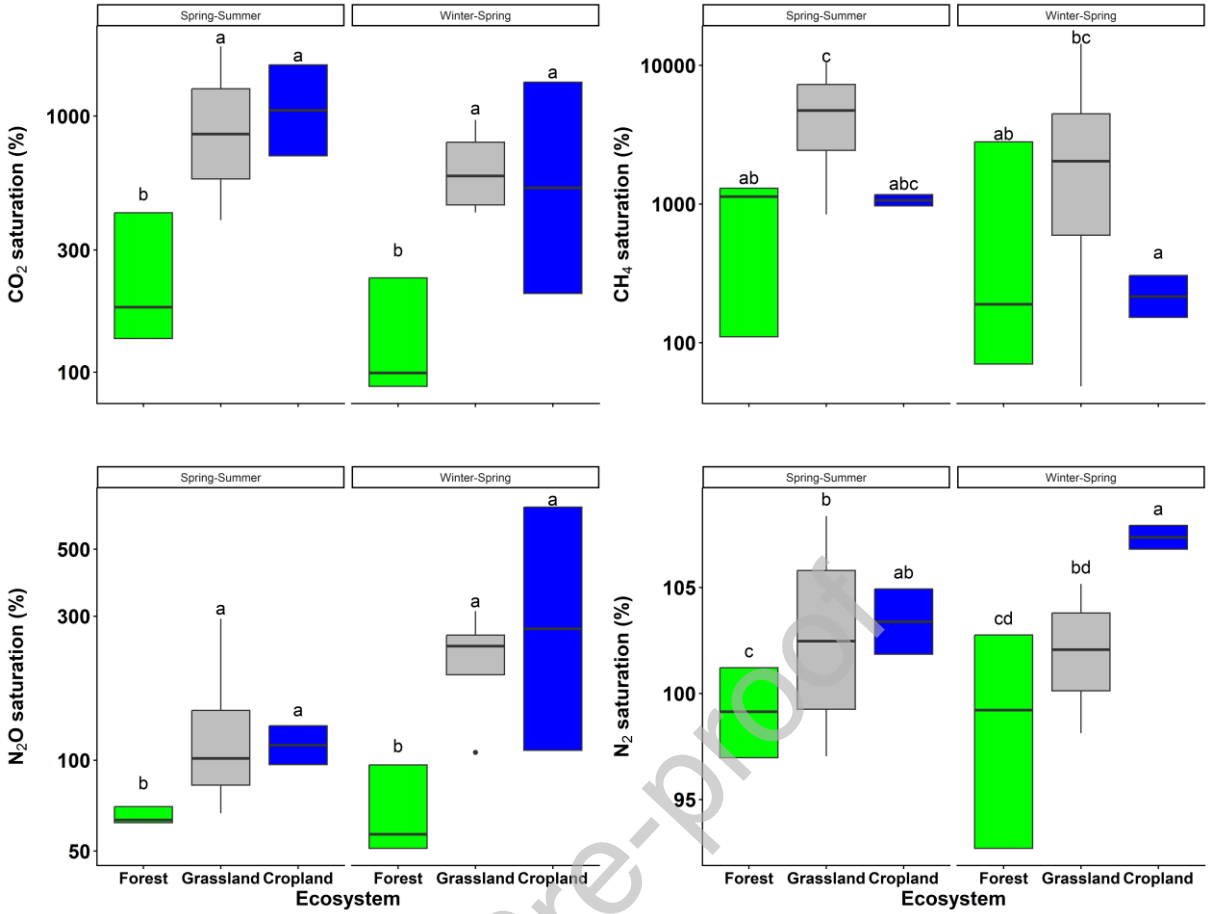

Figure 4: Seasonal and land use patterns of open channel CO_2, CH_4, N_2O, and N_2 saturation and fluxes across nine sites (forest=3, grassland = 4, cropland =2). Differences indicated by the letters on top of the boxplots represent significant ($p < 0.05$) combined differences across seasons and land use, based on the non-parametric post-hoc Dunn's test.

3.4 Variability in sediment characteristics and their links to in-vitro N turnover rates, GHG, and N_2 saturation

While sediment textures were not quantitatively determined, field observations during sediment sampling indicated that they were mainly a mixture of gravel and fine sediments, but the dominance of either varied across sites. Elemental analysis revealed that the carbon content, nitrogen content, and $\delta^{15}N$ isotopic signatures of sediments across the nine sampled sites varied widely, ranging from 3.1 to 12.4% C, 0.05 to 0.18% N, and -0.68 to 7.54‰, respectively (Table S3; Figure S2). As with other measured parameters, land use significantly influenced sediment characteristics (Figure S2). Sediment $\delta^{15}N$ isotopic signatures were more variable in grassland streams compared to cropland and forested streams, ranging from 1.9 to 7.54‰ (Figure S2). Sediments within cropland streams had significantly higher N content, lower C content, lower C:N ratios, and their $\delta^{15}N$ were, on average, 4.81‰ enriched compared to forested streams, whose $\delta^{15}N$ signals were mainly close to zero (Figure S2). The enrichment in the sediment $\delta^{15}N$ was also significantly positively related to the site-scale cumulative N turnover rates (GNR+GA+DN: $r^2 = 0.62$, $p < 0.05$), with the higher enrichment in the cropland and grassland sites coinciding with higher N cycling rates (Figure 5A). Similar significant positive relationships were also found between sediment $\delta^{15}N$ enrichment and CO_2, N_2O, and N_2 saturation (Figure 5B, D, and E: $r^2 = 0.38 - 0.51$, $p < 0.05$). The relationship

with CH_4 saturation also showed a positive trend, although it was not statistically significant (Figure 5C, p >0.05).

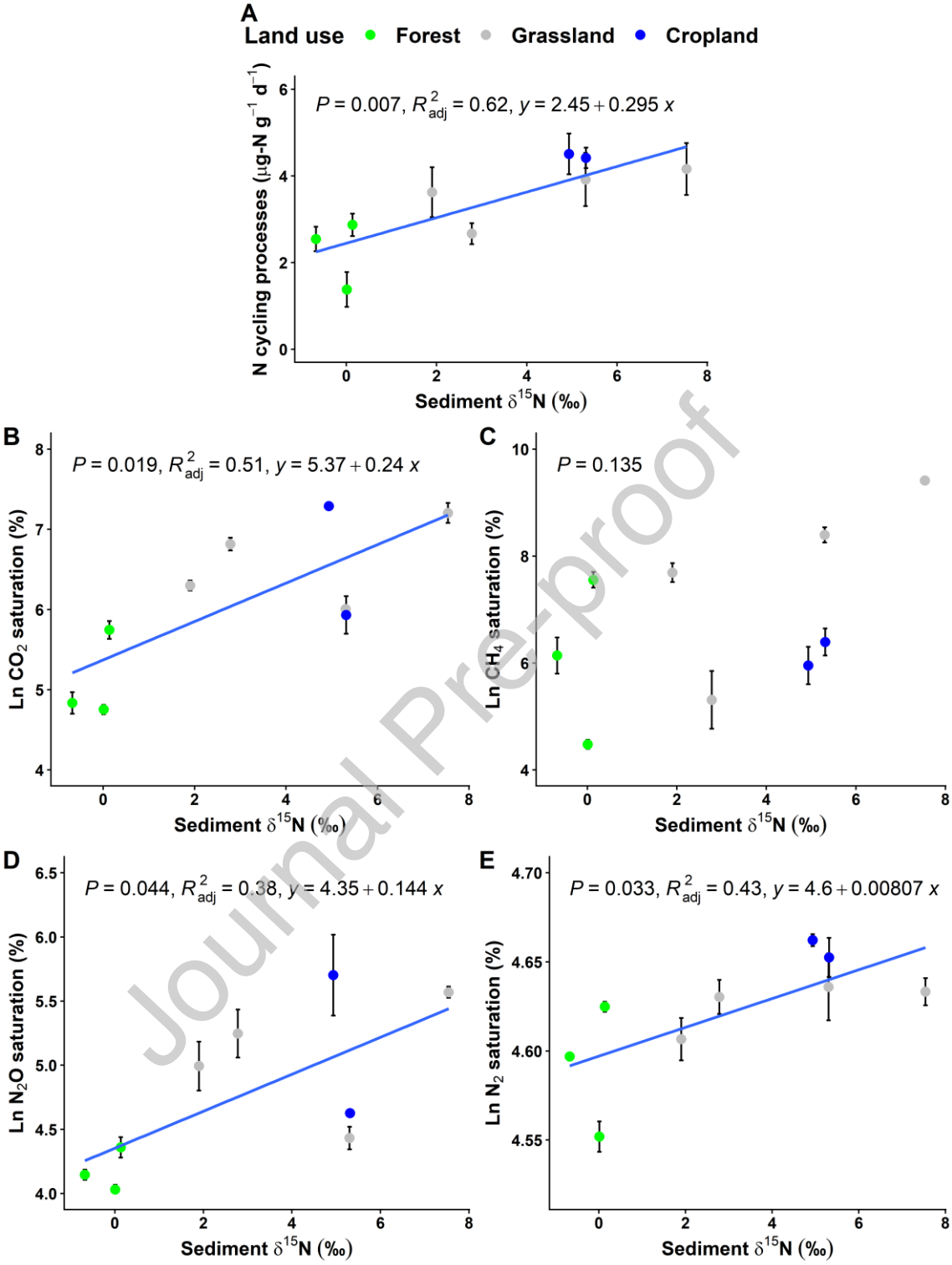

Figure 5: Bivariate relationship between sediment $\delta^{15}N$ (‰) and A) cumulative in-vitro N cycling rates (gross ammonification, gross nitrification, and denitrification), B) CO_2 saturation, C) CH_4 saturation, D N_2O saturation, and E) N_2 saturation. All GHG and N_2 saturation values are transformed with the natural logarithm. Points represent site-scale means ± SE, while the colors indicate the three main land use classes. The blue line represents the regression line, along with the equation, p-value, and adjusted R^2 value of the relationship.

3.5 Relationships between GHG and N_2 saturation with agricultural land use, sediment $\delta^{15}N$, in-vitro N cycling processes, and other key water quality parameters

In addition to assessing general land use and seasonal patterns in GHG and N_2 dynamics, we also evaluated site-scale variation associated with differences in upstream agricultural land use (% grassland + cropland), sediment $\delta^{15}N$, in-vitro nitrogen cycling rates, and key water-quality parameters (Figure 6). Based on the coefficient of determination (R^2) from the elastic-net regression models, these predictors explained far more variance in GHG (R^2 = 0.64 – 0.88) saturation than in N_2 (R^2 = 0.46). Among the environmental integrator variables, the percent of agricultural land use within the catchments was positively associated with CO_2, CH_4, N_2O, and N_2 saturation (Figure 6). However, its influence was comparatively less than that of sediment $\delta^{15}N$, which also exhibited positive relationships with CO_2, CH_4, and N_2 saturation and emerged as one of the strongest predictor variables based on effect sizes (Figure 6). For the water-quality predictor variables, DO saturation was negatively associated with CO_2, N_2O, and N_2 saturation (Figure 6). DIN and DON concentrations were generally positively related to GHG and N_2 saturation. Notably, DIN was most strongly associated with N_2O and N_2 oversaturation, whereas DON had stronger positive relationships with N_2O and CH_4 oversaturation (Figure 6). In contrast, DOC showed only weak positive relationships with CO_2, CH_4, and N_2 saturation, and was not related to N_2O.

In vitro N-cycling processes also broadly aligned with in situ GHG and N_2 saturation patterns (Figure 6). Gross nitrification rates were positively related to all three GHGs and N_2, with the strongest effects observed for N_2 saturation. In-vitro denitrification rates showed mixed relationships, being positive with CO_2, CH_4, and N_2 saturation, but negative with N_2O saturation. Gross ammonification rates were positively related to CH_4 saturation and negatively related to N_2 saturation, but had no relationships with CO_2 or N_2O. Overall, across the predictors, site-scale variation in CO_2 saturation was most strongly explained by environmental variables, especially sediment $\delta^{15}N$. Dissolved nitrogen concentrations were primarily linked to N_2O saturation, whereas N_2 saturation was best predicted by in-vitro N-cycling rates. CH_4 saturation showed mixed responses and was mainly influenced by all types of predictors.

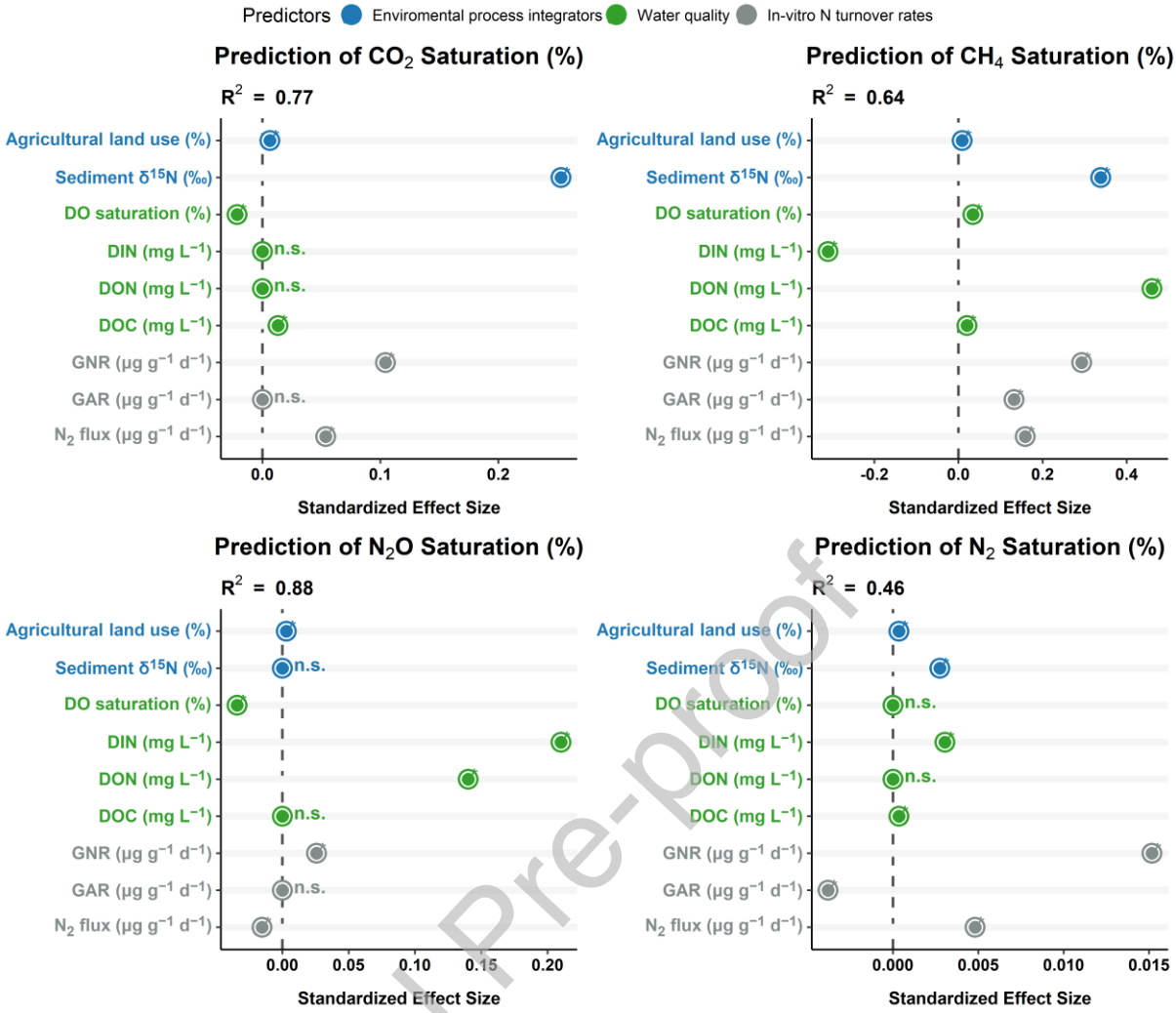

Figure 6: Results from elastic net regression models showing relationships of key site-scale parameters, including environmental process integrators, water quality, and in-vitro N turnover rates with natural log transformed open channel CO_2, CH_4, N_2O, and N_2 saturations (%). The points represent standardized effect sizes (positive or negative), with important relationships indicated by * (non-zero coefficients) and (n.s.) (zero coefficients). Color differences represent the three predictor groups.

4. Discussions

This study presented a comprehensive dataset that integrates current nitrogen turnover processes with sediment $\delta^{15}N$, a long-term indicator of nitrogen cycling. The main aim was to provide a mechanistic understanding of how differences in nitrogen availability across various land uses influence fluvial GHG emissions and denitrification losses. Consistent with previous research, streams within fertilized croplands or grasslands had much higher GHG emissions and denitrification N losses than forested streams across both seasons (Arango & Tank, 2008; Borges et al., 2018; Mwanake et al., 2023a). Cropland streams in particular were also characterized by lower carbon-to-nitrogen (C:N) ratios in both the sediment and water column (Figure S2), probably linked to significant long-term nitrogen inputs from the surrounding terrestrial landscapes related to synthetic N-based fertilizer additions (e.g., Wachholz et al., 2023). Declines in in-stream C:N ratios have been shown to promote microbial processes that may enhance GHG and N_2 production (Helton et al., 2015; Taylor & Townsend, 2010), which may explain our overall findings in this study. However, unlike earlier studies that largely inferred such processes (e.g., Bodmer et al., 2016; Herreid et al., 2021; Mwanake et al., 2023a), this study directly quantified them using stable isotope techniques. For instance, N turnover processes quantified from ^{15}N enrichment experiments were up to three times higher in cropland and grassland streams than in forested streams. These nitrogen turnover processes also exhibited predominantly positive relationships with open-channel CO_2, CH_4, N_2O, and N_2 oversaturation (Figure 6), suggesting either direct links to gaseous nitrogen losses or indirect associations mediated by co-occurring conditions, such as the availability of nitrogen-rich, labile organic carbon that may promote gaseous carbon losses (Figure 6).

The role of synthetic nitrogen fertilizer in driving stream N pollution was also implied by the $\delta^{15}N$-DIN isotopic values, which are commonly used to trace nitrogen sources in aquatic ecosystems (e.g., Duan et al., 2021; Wong et al., 2018). In particular, the highest DIN concentrations (mainly NO_3-N), observed in cropland streams during the winter–spring transition, were associated with the most depleted $\delta^{15}N$-DIN signatures, consistent with isotopic patterns characteristic of synthetic N-based fertilizer (Choi et al., 2017). The linear relationship of the Keeling plot also possibly indicated the conservative mixing of nitrate sources with different isotopic signatures, as opposed to fractionation processes like denitrification, which would produce non-linear relationships (Robinson & Conroy, 1998). These source-mixing dynamics may have been specific to the watersheds in this study, where dilution effects during the winter-spring snowmelt period and competing DIN sources may have dominated the observed isotopic composition across the land-use gradient.

Overall, these findings suggest potential links between intensified fluvial nitrogen turnover in human-impacted ecosystems and enhanced fluvial GHG emissions and denitrification losses under elevated nitrogen loading from surrounding terrestrial landscapes. We hypothesize that these anthropogenic effects may have been integrated into sediment $\delta^{15}N$ isotopic signals, which may reflect long-term elevated biogeochemical nitrogen cycling and losses in streams, as previously shown for soils (Craine et al., 2015; Wangari et al., 2024). This hypothesis was also supported by positive links between sediment $\delta^{15}N$ enrichment and GHG and N_2 oversaturation (Figure 5; Figure 6), as well as in-vitro N turnover rates (Figure 5A), suggesting that these hotspots may have persisted over long timescales (decades) due to excessive terrestrial N inputs. In addition to in-stream processing, sediment $\delta^{15}N$ isotopic signals may also reflect terrestrial sediment sources via inter-ecosystem transport (e.g., Riddle et al., 2025). Such sediment sources may be influenced by both terrestrial N turnover processes and N input sources, which differ in their $\delta^{15}N$ isotopic values (Choi et al., 2017; Denk et al., 2017). By integrating both instream processes with terrestrial-stream transport mechanisms, our findings demonstrate the potential of sediment $\delta^{15}N$ as an indicator of long-

term GHG emissions and nitrogen cycling hotspots in fluvial systems linked to both physical and biogeochemical processes.

4.1 Effects of seasonality and land use on fluvial N cycling processes

In terms of comparisons with existing values, the range of fluvial N cycling rates quantified here (0.02 to 5.4 μg g^{-1} d^{-1}) falls within the range of past studies (0.05 to 25.8 μg g^{-1} d^{-1}) (Arango & Tank, 2008; Lin et al., 2017, 2021; Vincent et al., 2025; X. Xu et al., 2025). Across the two sampled seasons, gross nitrification and ammonification rates were approximately nine times higher than their corresponding net rates (Table S3). Such a finding indicated that relying solely on net rate measurements may substantially underestimate nitrogen cycling in fluvial ecosystems. This underestimation aligns with findings from terrestrial systems, where similar discrepancies between gross and net rates have been observed (Verchot et al., 2001). However, such comparisons have rarely been demonstrated for fluvial environments, which have traditionally depended on indirect estimates through nitrification inhibition assays (e.g., Arango & Tank, 2008; Strauss & Lamberti, 2002; Vincent et al., 2025).

We also found that using only net rates may obscure important differences in N turnover process rates integrated in land use or seasonal differences. For instance, both gross nitrification and gross ammonification rates were up to 3 times higher in cropland streams than in forested streams, mirroring patterns in DIN concentrations (Figure 2; Figure 3). Such findings suggest elevated nitrogen turnover under N-rich instream conditions associated with upstream cropland land use (e.g., Arango & Tank, 2008; Beaulieu et al., 2011). In contrast, these land use differences were less apparent in the net rates (Figure S1).

The influence of external DIN inputs was also evident when comparing land use differences in gross N turnover rates and denitrification losses (Figure 3; Table S4). Across both seasons, gross nitrification rates in cropland streams were up to 3.6 times higher than gross ammonification rates. However, in grassland and forested streams, they were lower or only slightly higher (Figure 3; Table S4). This pattern suggests that nitrification rates in cropland streams were supported by external NH_4-N inputs not derived from internal mineralization. This was mainly evident during the spring–summer transition, when the discrepancy between the two rates was greatest (Table S4). During the same period, denitrification N losses in cropland streams were also up to seven times higher than the mean gross N transformation rates in grassland and forested streams. This finding suggests substantial external NO_3-N inputs that may have fueled enhanced denitrification activity in these ecosystems. Although the contribution of external DIN to increased in-stream nitrogen cycling has been inferred in previous studies (e.g., Mwanake et al., 2019, 2022, 2023a; Upadhyay et al., 2023; W. Xu et al., 2024), very few have provided quantitative evidence (e.g., Arango & Tank, 2008; Beaulieu et al., 2011). Our findings, therefore, suggest that combining direct measurements of N turnover rates can provide more substantial evidence for the influence of terrestrial nitrogen inputs on stream N dynamics and gaseous losses (e.g., Arango & Tank, 2008; Beaulieu et al., 2011; Vincent et al., 2025).

Several studies have linked elevated nitrification rates to ammonium availability based on bivariate relationships (Arango & Tank, 2008; Strauss et al., 2002; Strauss & Lamberti, 2002; Vincent et al., 2025), but not through the direct quantification of ammonification rates in streams. However, in this study, we show possible direct links between elevated gross ammonification rates and gross nitrification rates during the winter-spring transition in agricultural streams, suggesting that the decrease in the NH_4-N demand of photoautotrophs during this period may have promoted ammonification-driven nitrification rates (Figure 3). The reduction in photoautotrophic N uptake in winter may also have been reflected in the

overall depleted δ^{15}N-DIN values during this period (Figure S3), suggesting reduced isotopic enrichment from this process and thereby preserving the isotopic signature of the dominant N source. These N sources may include synthetic fertilizers for cropland streams, manure inputs for grassland streams, and mineralized leaf litter for forested streams, as reflected in their δ^{15}N-DIN isotopic signatures: depleted for cropland streams and enriched for grassland and forested streams (Choi et al., 2017). In contrast to gross nitrification and ammonification rates, denitrification rates were higher in cropland streams during the spring-summer transition than the winter-spring transition, suggesting a higher temperature sensitivity of the process or higher nitrate inflows. These findings also agree with a global meta-analysis on controls of denitrification in aquatic ecosystems, which linked a combination of higher temperatures and spring nitrate inflows to high denitrification rates during the summer (Piña-Ochoa & Álvarez-Cobelas, 2006).

Overall, while land use had a strong influence on fluvial N turnover rates, the general seasonal effects were not as evident, given a temperature difference of ~5°C between the two seasonal transition periods studied. This lack of strong seasonal effects may suggest that either land use integrates better site-scale differences in nitrogen turnover rates or that the temperature variation in this study was insufficient to drive significant biogeochemical seasonal differences. We hypothesize that both reasons may explain our findings. For example, going by the patterns discussed above, land use seems to be an essential integrator of fluvial nitrogen turnover trends, which may also modulate seasonal "hot moments," given the strong dependence of these processes on land use-driven nitrogen availability (e.g., Arango & Tank, 2008; Beaulieu et al., 2011; Vincent et al., 2025). However, numerous studies have also shown substantial temporal variability in GHG emissions or denitrification rates (Koschorreck et al., 2024; Manis et al., 2014; Mwanake et al., 2023a; Nevorski & Marcarelli, 2022; Piatka et al., 2024), likely reflecting similar changes in their underlying biogeochemical processes. Based on these studies, the temporal dynamics in GHG or denitrification rates were linked to short-term biogeochemical cycles, discharge fluctuations, and seasonal changes in temperature and precipitation. Consequently, our coarse sampling approach, which captures only two transition periods, likely underestimated the temporal variability in N-turnover processes due to similar drivers. Such an underestimation may have been larger in human-influenced streams, where biogeochemical process fluctuations are likely more pronounced due to elevated temporal substrate dynamics (e.g., B. Liu et al., 2023; Mwanake et al., 2023a).

4.2 Effects of seasonality and land use on the riverine GHG emissions and open channel denitrification.

Streams in this study primarily acted as net sources of GHGs and N_2 to the atmosphere, underscoring their dual role as both emitters of GHGs and key ecological agents that remove excess nitrogen through denitrification (Lauerwald et al., 2023a; X. Xu et al., 2025). Moreover, the ranges of stream GHG fluxes quantified during the two transitional periods are within those reported for temperate ecosystems and global ranges (Lauerwald et al., 2023b). While field measurements of fluvial GHG fluxes have increased in recent years, open-channel N_2 flux data are still scarce (e.g., Mwanake et al., 2024; Pribyl et al., 2005; Reisinger et al., 2016), with most current estimates of denitrification based on upscaled fluxes from sediment assays with the acetylene inhibition method (e.g., Kreiling et al., 2019; Qi & Liu, 2023; X. Xu et al., 2025; Yang et al., 2021). In comparison to these available datasets, the open channel N_2 flux data here fall within the same order of magnitude as the range of past global estimates quantified from different methodologies (0 – 27.84 g N_2 m^{-2} d^{-1} from Table 2 in Yang et al., 2021), but is higher than the current open channel estimates (− 1.7 to

6.16 g N_2 m^{-2} d^{-1}), primarily conducted in large rivers with lower water-air gas exchange rates (Mwanake et al., 2024; Pribyl et al., 2005; Reisinger et al., 2016).

In terms of land use differences, streams located in cropland and grassland areas exhibited higher GHG emissions and open-channel denitrification rates compared to forested streams, aligning with findings from previous studies in temperate ecosystems (Arango & Tank, 2008; Beaulieu et al., 2011; Mwanake et al., 2025a). Relative to natural ecosystems, agricultural streams, particularly those within cropland areas, may have elevated N and more N-rich bioavailable carbon supplies, which may enhance GHG production processes such as respiration, methanogenesis, nitrification, and denitrification (See Drake et al., 2019; Masese et al., 2017; Mulholland et al., 2009; Vincent et al., 2025). The results of this study suggest similar mechanisms that may underlie the observed land use patterns, linking carbon and nitrogen cycling. For example, cropland and grassland streams in this study mainly exhibited lower DO saturations and higher concentrations of DON and DIN, conditions indicative of enhanced biogenic activity driven by increased carbon and nitrogen bioavailability (e.g., Graeber et al., 2015). We also observed strong positive correlations between DON (more bioavailable DOM) and N_2O and CH_4 saturation, as well as between DIN and N_2O and N_2 saturation. In contrast, DO showed negative correlations with both CO_2 and N_2O saturation. Overall, these findings suggest the possible enhancement of instream CO_2, CH_4, and N_2O production rates under elevated N conditions (e.g., Borges et al., 2018; Mwanake et al., 2023a; Upadhyay et al., 2023; Battin et al., 2023).

Using in-vitro process-based measurements, we further inferred possible links between intensified biogeochemical N cycling and elevated riverine GHG and N_2 oversaturation (Figure 6). Specifically, instream CO_2, CH_4, and N_2 saturations were positively related to in-vitro denitrification rates, consistent with previous findings that associate elevated respiration with increased denitrification due to favorable reducing redox conditions (Helton et al., 2015; Mulholland et al., 2009; Reisinger et al., 2016). On the other hand, N_2O saturations were negatively related to in-vitro denitrification rates, consistent with the expected reduction of N_2O to N_2 through complete denitrification. In contrast, all three GHGs and N_2 saturations were also positively related to gross nitrification rates, suggesting either direct links between the process and N_2O and N_2 saturation, or indirect links with co-occurring conditions, such as elevated N-rich labile carbon sources, that may promote CO_2 and CH_4 production, as discussed above.

Previous fluvial research has inferred links between elevated instream NO_3-N concentrations and increased N_2O or N_2 production, primarily through bivariate relationships (Baulch et al., 2011; Beaulieu et al., 2011; Mulholland et al., 2009; Mwanake et al., 2019; J. Wang et al., 2022). However, only a handful of studies have explored such links using direct measurements of nitrification-driven N_2O or N_2 fluxes in streams (Ouyang et al., 2021; S. Wang et al., 2024). Quantifying actual nitrification rates, understanding their controls, and examining their relationship to gaseous nitrogen losses are essential, as these processes can affect the N_2O:N_2 ratio, which is crucial for determining whether fluvial ecosystems serve as sources or sinks of N_2O. The importance of direct process-based measurements was demonstrated in a recent study, which found initial evidence that elevated instream CO_2 stimulated gross nitrification rates, possibly enhancing N_2O production in river ecosystems (Mwanake et al., 2025b). We hypothesize that a similar mechanism may explain the positive relationship that we found between CO_2 concentrations and N_2O:N_2 saturation ratios (Figure S5). However, this correlation does not necessarily imply causality, and further experimental studies are needed to strengthen the potential biogeochemical linkages between CO_2 and N_2O in rivers.

4.3 Sediment $\delta^{15}N$ as an indicator of long-term riverine denitrification and GHG emission hotspots

Natural abundance $\delta^{15}N$ isotopic signatures in soils and sediments are widely recognized as integrators of long-term nitrogen cycling (Diebel & Zanden, 2009; Wangari et al., 2024; Liao et al., 2021; Peipoch et al., 2012). In terrestrial ecosystems, enriched $\delta^{15}N$ values have been hypothesized to typically reflect a more open nitrogen cycle characterized by substantial nitrogen inputs, turnover, and losses (e.g., Craine et al., 2015; Wangari et al., 2024). Mechanistically, elevated N turnover process rates result in higher isotopic fractionation, where microbes preferentially uptake the lighter ^{14}N isotopes over the heavier ^{15}N isotopes, producing ^{15}N-depleted products while leaving the remaining substrate pool progressively enriched in ^{15}N (Craine et al., 2015). This fractionation and subsequent enrichment also depend on the dominating process, and can range widely for key processes such as nitrification and denitrification (Denk et al., 2017).

In this study, sediment $\delta^{15}N$ values were more enriched in grassland and cropland streams than in forested streams (Figure S2), suggesting a similar mechanism: a more open nitrogen cycle in these ecosystems characterized by the same processes. This hypothesis was further supported by the positive correlations between sediment $\delta^{15}N$ enrichment and rates of nitrogen cycling processes (Figure 5A). Such findings may indicate that land use intensification due to fertilization likely affects the level of nitrogen inputs to rivers, which in turn influences in-stream biogeochemical processes (e.g., Mwanake et al., 2025c). Because sediment $\delta^{15}N$ enrichment reflects sites with elevated long-term nitrogen inputs, cycling, and loss rates, we also examined whether these locations align with current open channel GHG and denitrification rates. Our results showed proportional increases in open-channel CO_2, CH_4, N_2O, and N_2 oversaturation with increasing sediment $\delta^{15}N$ enrichment (Figure 5), suggesting linkages between fluvial carbon and nitrogen gaseous losses and enhanced in-stream nitrogen cycling under human influence. We contend that the relationships between sediment $\delta^{15}N$ enrichment and hotspots of nitrogen gaseous losses are likely more direct, reflecting enhanced rates of coupled in-stream nitrification-denitrification that drive long-term isotopic fractionation in sediments similar to soils (e.g., Wangari et al., 2024). In contrast, the found links between gaseous carbon losses (CO_2 and CH_4) and sediment $\delta^{15}N$ enrichment suggest indirect linkages, possibly arising from co-occurring conditions in human-impacted streams, including greater availability of nitrogen-rich, labile organic carbon (e.g., Upadhyay et al., 2023). Such conditions can stimulate heterotrophic respiration and methanogenesis, thereby increasing CO_2 and CH_4 oversaturation (See Drake et al., 2019; Stanley et al., 2016). Taken together, these findings underscore the potential of sediment $\delta^{15}N$ as an integrative indicator for tracking long-term anthropogenic nitrogen inputs and their coupled effects on fluvial greenhouse gas emissions and denitrification-related N losses.

5. Conclusions

Agricultural activities are well known to influence fluvial greenhouse gas (GHG) emissions and denitrification losses; however, the underlying mechanisms remain uncertain. In this study, we combined direct measurements of nitrogen (N) cycling rates with field observations of GHG emissions and N_2 fluxes across streams exhibiting different levels of agriculture-linked N pollution. We found potential links between elevated N cycling rates and both GHG and denitrification hotspots, with these processes scaling well with increasing agricultural land use. In addition, both sediment and water-column $\delta^{15}N$ isotopic signatures seemed to be potential indicators of short- and long-term anthropogenic N pollution, possibly reflecting enhanced fertilizer inputs and higher long-term N turnover rates. As such, we argue that such hotspots may be potential targets for future ecological management strategies, aimed at maximizing fluvial denitrification N_2 losses while minimizing their CO_2, CH_4, and N_2O

emissions. Based on results from this and other studies, management interventions should prioritize preserving natural forest ecosystems while reducing excess nitrogen inputs to streams draining agricultural areas. For instance, synchronizing fertilization timing with periods of maximum plant nitrogen uptake may enhance nitrogen use efficiency of farming systems and minimize losses to streams. Alternatively, the reduction of terrestrial-stream nitrogen transfer during periods of hydrological connectivity can also be achieved through the restoration of wide riparian forest buffers. These integrative strategies are likely to result in closed fluvial N cycles, with minimal adverse environmental impacts.

Nevertheless, our study was not without limitations that represent promising directions for future research. While our findings demonstrate strong correlations that support the hypothesis that sediment $\delta^{15}N$ can serve as a proxy for long-term N-cycling hotspots, it is crucial to note that this study establishes association, not causation. Future manipulative experiments are needed to confirm the causal links proposed here. Our study was also based on a relatively coarse spatial and temporal sampling regime, focusing on only a few sites and two transition periods in the temperate region, which likely missed key short-term "hot moments" or spatial hotspots of fluvial N cycling rates. Such data gaps may have influenced the positive relationship we observed between sediment $\delta^{15}N$ and nitrogen cycling, which may have been stronger if spatial and temporal variability in N cycling processes had been better captured. Future work should incorporate higher-temporal frequency process measurements across diverse climatic regions to better constrain how agricultural practices shape fluvial GHG emissions and denitrification by altering instream biogeochemical dynamics. Moreover, our study design was also unable to determine whether the sediment $\delta^{15}N$ enrichment reflected instream cycling rates alone or physical sediment transport between streams and their surrounding terrestrial environments. Future research should strive to make this partition, as such information will be highly critical for informing future mitigation strategies more effectively, which may be specific to lowering instream biogeochemical rates or stream-terrestrial interactions.

Author contributions

RMM and RK conceived this study. RMM, MA, HM performed the field research. RMM, EGW, AK, MA, and HM performed the laboratory analysis. RMM and RK designed the data analysis strategies. RMM and EGW analyzed the data. RMM wrote the first draft, with contributions from all authors for the preparation of the final draft.

Funding

Infrastructure for the research was provided by the TERENO Bavarian Alps/Pre-Alps Observatory, funded by the Helmholtz Association through the joint program Changing Earth – Sustaining our Future (ATMO - PoF IV) program of Karlsruhe Institute of Technology (KIT).

Declaration of competing interests

The authors declare that they have no known competing financial interests or personal relationships that could have appeared to influence the work reported in this paper.

Data availability

The raw dataset for this manuscript is publicly available for download at https://doi.org/10.5281/zenodo.17768138

References

Ågren, A., Haei, M., Köhler, S. J., Bishop, K., & Laudon, H. (2010). Regulation of stream water dissolved organic carbon (DOC) concentrations during snowmelt; the role of discharge, winter climate and memory effects. *Biogeosciences*, *7*(9), 2901–2913. https://doi.org/10.5194/bg-7-2901-2010

Aho, K. S., & Raymond, P. A. (2019). Differential response of greenhouse gas evasion to storms in forested and wetland streams. *Journal of Geophysical Research: Biogeosciences*, *124*(3), 649-662. https://doi.org/10.1029/2018JG004750

Aho, K. S., Fair, J. H., Hosen, J. D., Kyzivat, E. D., Logozzo, L. A., Rocher-Ros, G., Weber, L. C., Yoon, B., & Raymond, P. A. (2021). Distinct concentration-discharge dynamics in temperate streams and rivers: CO2 exhibits chemostasis while CH4 exhibits source limitation due to temperature control. *Limnology and Oceanography*, *66*(10), 3656–3668. https://doi.org/10.1002/lno.11906

Arango, C. P., & Tank, J. L. (2008). Land use influences the spatiotemporal controls on nitrification and denitrification in headwater streams. *Journal of the North American Benthological Society*, *27*(1), 90–107. https://doi.org/10.1899/07-024.1

Battin, T. J., Lauerwald, R., Bernhardt, E. S., Bertuzzo, E., Gener, L. G., Hall, R. O., Hotchkiss, E. R., Maavara, T., Pavelsky, T. M., Ran, L., Raymond, P., Rosentreter, J. A., & Regnier, P. (2023). River ecosystem metabolism and carbon biogeochemistry in a changing world. *Nature*, *613*(7944), 449–459. https://doi.org/10.1038/s41586-022-05500-8

Beaulieu, J. J., Tank, J. L., Hamilton, S. K., Wollheim, W. M., Hall, R. O., Mulholland, P. J., Peterson, B. J., Ashkenas, L. R., Cooper, L. W., Dahm, C. N., Dodds, W. K., Grimm, N. B., Johnson, S. L., McDowell, W. H., Poole, G. C., Maurice Valett, H., Arango, C. P., Bernot, M. J., Burgin, A. J., … Thomas, S. M. (2011). Nitrous oxide emission from denitrification in stream and river networks. *Proceedings of the National Academy of Sciences of the United States of America*, *108*(1), 214–219. https://doi.org/10.1073/pnas.1011464108

Bellmore, R. A., Compton, J. E., Brooks, J. R., Fox, E. W., Hill, R. A., Sobota, D. J., Thornbrugh, D. J., & Weber, M. H. (2018). Nitrogen inputs drive nitrogen concentrations in U.S. streams and rivers during summer low flow conditions. *Science of The Total Environment*, *639*, 1349–1359. https://doi.org/10.1016/j.scitotenv.2018.05.008

Bodmer, P., Heinz, M., Pusch, M., Singer, G., & Premke, K. (2016). Carbon dynamics and their link to dissolved organic matter quality across contrasting stream ecosystems. *Science of the Total Environment*, *553*, 574–586. https://doi.org/10.1016/j.scitotenv.2016.02.095

Borges, A. V., Darchambeau, F., Lambert, T., Bouillon, S., Morana, C., Brouyère, S., Hakoun, V., Jurado, A., Tseng, H. C., Descy, J. P., & Roland, F. A. E. (2018). Effects of agricultural land use on fluvial carbon dioxide, methane and nitrous oxide concentrations in a large European river, the Meuse (Belgium). *Science of the Total Environment*, *610–611*, 342–355. https://doi.org/10.1016/j.scitotenv.2017.08.047

Brookshire, E. N. J., Valett, H. M., Thomas, S. A., & Webster, J. R. (2005). COUPLED CYCLING OF DISSOLVED ORGANIC NITROGEN AND CARBON IN A FOREST STREAM. *Ecology*, *86*(9), 2487–2496. https://doi.org/10.1890/04-1184

Choi, W. J., Kwak, J. H., Lim, S. S., Park, H. J., Chang, S. X., Lee, S. M., Arshad, M. A., Yun, S. I., & Kim, H. Y. (2017). Synthetic fertilizer and livestock manure differently affect δ15N in the agricultural landscape: A review. In *Agriculture, Ecosystems and Environment* (Vol. 237, pp. 1–15). Elsevier B.V. https://doi.org/10.1016/j.agee.2016.12.020

Craine, J. M., Brookshire, E. N. J., Cramer, M. D., Hasselquist, N. J., Koba, K., Marin-Spiotta, E., & Wang, L. (2015). Ecological interpretations of nitrogen isotope ratios of terrestrial plants and soils. In *Plant and Soil* (Vol. 396, Issues 1–2, pp. 1–26). Springer International Publishing. https://doi.org/10.1007/s11104-015-2542-1

Denk, T. R. A., Mohn, J., Decock, C., Lewicka-Szczebak, D., Harris, E., Butterbach-Bahl, K., Kiese, R., & Wolf, B. (2017). The nitrogen cycle: A review of isotope effects and isotope modeling approaches. *Soil Biology and Biochemistry*, *105*, 121–137. https://doi.org/10.1016/j.soilbio.2016.11.015

Diebel, M. W., & Zanden, M. J. Vander. (2009). Nitrogen stable isotopes in streams: effects of agricultural sources and transformations. *Ecological Applications*, *19*(5), 1127–1134. https://doi.org/10.1890/08-0327.1

Drake, T. W., Van Oost, K., Barthel, M., Bauters, M., Hoyt, A. M., Podgorski, D. C., Six, J., Boeckx, P., Trumbore, S. E., Cizungu Ntaboba, L., & Spencer, R. G. M. (2019). Mobilization of aged and biolabile soil carbon by tropical deforestation. *Nature Geoscience*, *12*(7), 541–546. https://doi.org/10.1038/s41561-019-0384-9

Duan, S., Kaushal, S. S., Rosenfeldt, E. J., Huang, J., & Murthy, S. (2021). Changes in concentrations and source of nitrogen along the Potomac River with watershed land use. *Applied Geochemistry*, *131*, 105006. https://doi.org/10.1016/j.apgeochem.2021.105006

Farr, T. G., Rosen, P. A., Caro, E., Crippen, R., Duren, R., Hensley, S., Kobrick, M., Paller, M., Rodriguez, E., Roth, L., Seal, D., Shaffer, S., Shimada, J., Umland, J., Werner, M., Oskin, M., Burbank, D., & Alsdorf, D. (2007). The Shuttle Radar Topography Mission. *Reviews of Geophysics*, *45*(2). https://doi.org/10.1029/2005RG000183

Fasching, C., Akotoye, C., Bižić, M., Fonvielle, J., Ionescu, D., Mathavarajah, S., Zoccarato, L., Walsh, D. A., Grossart, H., & Xenopoulos, M. A. (2020). Linking stream microbial community functional genes to dissolved organic matter and inorganic nutrients. *Limnology and Oceanography*, *65*(S1). https://doi.org/10.1002/lno.11356

Wangari, E.G, Mwanake, R. M., Houska, T., Kraus, D., Kikowatz, H.-M., Wolf, B., Gettel, G. M., Breuer, L., Ambus, P., Kiese, R., & Butterbach-Bahl, K. (2024). Spatial-temporal patterns of foliar and bulk soil 15N isotopic signatures across a heterogeneous landscape: Linkages to soil N status, nitrate leaching, and N2O fluxes. *Soil Biology and Biochemistry*, *199*, 109609. https://doi.org/10.1016/j.soilbio.2024.109609

Graeber, D., Boëchat, I. G., Encina-Montoya, F., Esse, C., Gelbrecht, J., Goyenola, G., Gücker, B., Heinz, M., Kronvang, B., Meerhoff, M., Nimptsch, J., Pusch, M. T., Silva,

R. C. S., Von Schiller, D., & Zwirnmann, E. (2015). Global effects of agriculture on fluvial dissolved organic matter. *Scientific Reports*, *5*. https://doi.org/10.1038/srep16328

Hall, G. H. (1984). Measurement of nitrification rates in lake sediments: Comparison of the nitrification inhibitors nitrapyrin and allylthiourea. *Microbial Ecology*, *10*(1), 25–36. https://doi.org/10.1007/BF02011592

Helton, A. M., Ardón, M., & Bernhardt, E. S. (2015). Thermodynamic constraints on the utility of ecological stoichiometry for explaining global biogeochemical patterns. *Ecology Letters*, *18*(10), 1049–1056. https://doi.org/10.1111/ele.12487

Herreid, A. M., Wymore, A. S., Varner, R. K., Potter, J. D., & McDowell, W. H. (2021). Divergent Controls on Stream Greenhouse Gas Concentrations Across a Land-Use Gradient. *Ecosystems*, *24*(6), 1299–1316. https://doi.org/10.1007/s10021-020-00584-7

Hu, M., Chen, D., & Dahlgren, R. A. (2016). Modeling nitrous oxide emission from rivers: a global assessment. *Global Change Biology*, *22*(11), 3566–3582. https://doi.org/10.1111/gcb.13351

Jones, M. W., Peters, G. P., Gasser, T., Andrew, R. M., Schwingshackl, C., Gütschow, J., Houghton, R. A., Friedlingstein, P., Pongratz, J., & Le Quéré, C. (2023). National contributions to climate change due to historical emissions of carbon dioxide, methane, and nitrous oxide since 1850. *Scientific Data*, *10*(1). https://doi.org/10.1038/s41597-023-02041-1

Kana, T. M., Darkangelo, Christina., Hunt, M. Duane., Oldham, J. B., Bennett, G. E., & Cornwell, J. C. (1994). Membrane Inlet Mass Spectrometer for Rapid High-Precision Determination of N2, O2, and Ar in Environmental Water Samples. *Analytical Chemistry*, *66*(23), 4166–4170. https://doi.org/10.1021/ac00095a009

Kelly, M. C., Zeglin, L. H., Husic, A., & Burgin, A. J. (2021). High Supply, High Demand: A Fertilizer Waste Release Impacts Nitrate Uptake and Metabolism in a Large River. *Journal of Geophysical Research: Biogeosciences*, *126*(12). https://doi.org/10.1029/2021JG006469

Kemp, M. J., & Dodds, W. K. (2002). The influence of ammonium, nitrate, and dissolved oxygen concentrations on uptake, nitrification, and denitrification rates associated with prairie stream substrata. *Limnology and Oceanography*, *47*(5), 1380–1393. https://doi.org/10.4319/lo.2002.47.5.1380

Koschorreck, M., Kamjunke, N., Koedel, U., Rode, M., Schuetze, C., & Bussmann, I. (2024). Diurnal versus spatial variability of greenhouse gas emissions from an anthropogenically modified lowland river in Germany. *Biogeosciences*, *21*(6), 1613–1628. https://doi.org/10.5194/bg-21-1613-2024

Kreiling, R. M., Richardson, W. B., Bartsch, L. A., Thoms, M. C., & Christensen, V. G. (2019). Denitrification in the river network of a mixed land use watershed: unpacking the complexities. *Biogeochemistry*, *143*(3), 327–346. https://doi.org/10.1007/s10533-019-00565-6

Lauerwald, R., Allen, G. H., Deemer, B. R., Liu, S., Maavara, T., Raymond, P., Alcott, L., Bastviken, D., Hastie, A., Holgerson, M. A., Johnson, M. S., Lehner, B., Lin, P., Marzadri, A., Ran, L., Tian, H., Yang, X., Yao, Y., & Regnier, P. (2023a). Inland Water

Greenhouse Gas Budgets for RECCAP2: 1. State-Of-The-Art of Global Scale Assessments. In *Global Biogeochemical Cycles* (Vol. 37, Issue 5). John Wiley and Sons Inc. https://doi.org/10.1029/2022GB007657

Lauerwald, R., Allen, G. H., Deemer, B. R., Liu, S., Maavara, T., Raymond, P., Alcott, L., Bastviken, D., Hastie, A., Holgerson, M. A., Johnson, M. S., Lehner, B., Lin, P., Marzadri, A., Ran, L., Tian, H., Yang, X., Yao, Y., & Regnier, P. (2023b). Inland Water Greenhouse Gas Budgets for RECCAP2: 2. Regionalization and Homogenization of Estimates. In *Global Biogeochemical Cycles* (Vol. 37, Issue 5). John Wiley and Sons Inc. https://doi.org/10.1029/2022GB007658

Liao, K., Lai, X., & Zhu, Q. (2021). Soil δ^{15} N is a better indicator of ecosystem nitrogen cycling than plant δ^{15} N: A global meta-analysis. *SOIL*, *7*(2), 733–742. https://doi.org/10.5194/soil-7-733-2021

Lin, X., Li, X., Gao, D., Liu, M., & Cheng, L. (2017). Ammonium Production and Removal in the Sediments of Shanghai River Networks: Spatiotemporal Variations, Controlling Factors, and Environmental Implications. *Journal of Geophysical Research: Biogeosciences*, *122*(10), 2461–2478. https://doi.org/10.1002/2017JG003769

Lin, X., Lu, K., Hardison, A. K., Liu, Z., Xu, X., Gao, D., Gong, J., & Gardner, W. S. (2021). Membrane inlet mass spectrometry method (REOX/MIMS) to measure 15N-nitrate in isotope-enrichment experiments. *Ecological Indicators*, *126*. https://doi.org/10.1016/j.ecolind.2021.107639

Liu, B., Wang, Z., Tian, M., Yang, X., Chan, C. N., Chen, S., Yang, Q., & Ran, L. (2023). Basin-Scale CO_2 Emissions From the East River in South China: Importance of Small Rivers, Human Impacts and Monsoons. *Journal of Geophysical Research: Biogeosciences*, *128*(1). https://doi.org/10.1029/2022JG007291

Liu, S., Kuhn, C., Amatulli, G., Aho, K., Butman, D. E., Allen, G. H., Lin, P., Pan, M., Yamazaki, D., Brinkerhoff, C., Gleason, C., Xia, X., & Raymond, P. A. (2022). *The importance of hydrology in routing terrestrial carbon to the atmosphere via global streams and rivers*. https://doi.org/10.1073/pnas.2106322119/-/DCSupplemental

Malone, J. P., Stevens, R. J., & Laughlin, R. J. (1998). Combining the 15N and acetylene inhibition techniques to examine the effect of acetylene on denitrification. *Soil Biology and Biochemistry*, *30*(1), 31–37. https://doi.org/10.1016/S0038-0717(97)00088-6

Manis, E., Royer, T. V., Johnson, L. T., & Leff, L. G. (2014). Denitrification in Agriculturally Impacted Streams: Seasonal Changes in Structure and Function of the Bacterial Community. *PLoS ONE*, *9*(8), e105149. https://doi.org/10.1371/journal.pone.0105149

Marwick, T. R., Tamooh, F., Ogwoka, B., Teodoru, C., Borges, A. V., Darchambeau, F., & Bouillon, S. (2014). Dynamic seasonal nitrogen cycling in response to anthropogenic N loading in a tropical catchment, Athi–Galana–Sabaki River, Kenya. *Biogeosciences*, *11*(2), 443–460. https://doi.org/10.5194/bg-11-443-2014

Masese, F. O., Salcedo-Borda, J. S., Gettel, G. M., Irvine, K., & McClain, M. E. (2017). Influence of catchment land use and seasonality on dissolved organic matter composition and ecosystem metabolism in headwater streams of a Kenyan river. *Biogeochemistry*, *132*(1–2), 1–22. https://doi.org/10.1007/s10533-016-0269-6

Mulholland, P. J., Hall, R. O., Sobota, D. J., Dodds, W. K., Findlay, S. E. G., Grimm, N. B., Hamilton, S. K., McDowell, W. H., O'Brien, J. M., Tank, J. L., Ashkenas, L. R., Cooper, L. W., Dahm, C. N., Gregory, S. V., Johnson, S. L., Meyer, J. L., Peterson, B. J., Poole, G. C., Valett, H. M., … Thomasn, S. M. (2009). Nitrate removal in stream ecosystems measured by 15N addition experiments: Denitrification. *Limnology and Oceanography*, *54*(3), 666–680. https://doi.org/10.4319/lo.2009.54.3.0666

Murphy, D. V, Recous, S., Stockdale, E. A., Fillery, I. R. P., Jensen, L. S., Hatch, D. J., & Goulding, K. W. T. (2003). Gross nitrogen fluxes in soil : theory, measurement and application of 15N pool dilution techniques. In *Advances in Agronomy* (Vol. 79, pp. 69–118). Academic Press. https://doi.org/https://doi.org/10.1016/S0065-2113(02)79002-0

Mwanake, R. M., Gettel, G. M., Aho, K. S., Namwaya, D. W., Masese, F. O., Butterbach-Bahl, K., & Raymond, P. A. (2019). Land Use, Not Stream Order, Controls N2O Concentration and Flux in the Upper Mara River Basin, Kenya. *Journal of Geophysical Research: Biogeosciences*, *124*(11), 3491–3506. https://doi.org/10.1029/2019JG005063

Mwanake, R. M., Gettel, G. M., Ishimwe, C., Wangari, E. G., Butterbach-Bahl, K., & Kiese, R. (2022). Basin-scale estimates of greenhouse gas emissions from the Mara River, Kenya: Importance of discharge, stream size, and land use/land cover. *Limnology and Oceanography*, *67*(8), 1776–1793. https://doi.org/10.1002/lno.12166

Mwanake, R. M., Gettel, G. M., Wangari, E. G., Butterbach-Bahl, K., & Kiese, R. (2023b). Interactive effects of catchment mean water residence time and agricultural area on water physico-chemical variables and GHG saturations in headwater streams. *Frontiers in Water*, *5*. https://doi.org/10.3389/frwa.2023.1220544

Mwanake, R. M., Gettel, G. M., Wangari, E. G., Butterbach-Bahl, K., & Kiese, R. (2025c). *The role of agricultural fertilization intensity on fluvial GHG fluxes from tropical and temperate catchments*. https://doi.org/10.1016/j.jenvman.2025.127782

Mwanake, R. M., Gettel, G. M., Wangari, E. G., Glaser, C., Houska, T., Breuer, L., Butterbach-Bahl, K., & Kiese, R. (2023a). Anthropogenic activities significantly increase annual greenhouse gas (GHG) fluxes from temperate headwater streams in Germany. *Biogeosciences*, *20*(16), 3395–3422. https://doi.org/10.5194/bg-20-3395-2023

Mwanake, R. M., Gettel, G. M., Wangari, E. G., Macharia, G., Martinez-Cuesta, R., Schulz, S., Schloter, M., Butterbach-Bahl, K., & Kiese, R. (2025b). *Elevated In-Stream CO2 Concentration Stimulates Net-N2O Production from Global Fluvial Ecosystems*. https://doi.org/10.2139/ssrn.5176087

Mwanake, R. M., Imhof, H. K., & Kiese, R. (2024). Divergent drivers of the spatial variation in greenhouse gas concentrations and fluxes along the Rhine River and the Mittelland Canal in Germany. *Environmental Science and Pollution Research*. https://doi.org/10.1007/s11356-024-33394-8

Mwanake, R. M., Wangari, E. G., Winkler, K., Gretchen, G. M., Butterbach-Bahl, K., & Kiese, R. (2025a). From data to insights: Upscaling riverine GHG fluxes in Germany with machine learning. *Science of The Total Environment*, *958*, 177984. https://doi.org/10.1016/j.scitotenv.2024.177984

Nevorski, K. C., & Marcarelli, A. M. (2022). High Daily and Year-Round Variability in Denitrification and Nitrogen Fixation in a Northern Temperate River. *Frontiers in Water*, *4*. https://doi.org/10.3389/frwa.2022.894554

Ouyang, L., Thamdrup, B., & Trimmer, M. (2021). Coupled nitrification and N2 gas production as a cryptic process in oxic riverbeds. *Nature Communications*, *12*(1). https://doi.org/10.1038/s41467-021-21400-3

Peipoch, M., Martí, E., & Gacia, E. (2012). Variability in δ ^{15} N natural abundance of basal resources in fluvial ecosystems: a meta-analysis. *Freshwater Science*, *31*(3), 1003–1015. https://doi.org/10.1899/11-157.1

Peterson, B. J., Wollheim, W. M., Mulholland, P. J., Webster, J. R., Meyer, J. L., Tank, J. L., Martí, E., Bowden, W. B., Valett, H. M., Hershey, A. E., McDowell, W. H., Dodds, W. K., Hamilton, S. K., Gregory, S., & Morrall, D. D. (2001). Control of Nitrogen Export from Watersheds by Headwater Streams. *Science*, *292*(5514), 86–90. https://doi.org/10.1126/science.1056874

Piatka, D. R., Nánási, R. L., Mwanake, R. M., Engelsberger, F., Willibald, G., Neidl, F., & Kiese, R. (2024). Precipitation fuels dissolved greenhouse gas (CO2, CH4, N2O) dynamics in a peatland-dominated headwater stream: results from a continuous monitoring setup. *Frontiers in Water*, *5*. https://doi.org/10.3389/frwa.2023.1321137

Piña-Ochoa, E., & Álvarez-Cobelas, M. (2006). Denitrification in Aquatic Environments: A Cross-system Analysis. *Biogeochemistry*, *81*(1), 111–130. https://doi.org/10.1007/s10533-006-9033-7

Plont, S., O'Donnell, B. M., Gallagher, M. T., & Hotchkiss, E. R. (2020). Linking carbon and nitrogen spiraling in streams. *Freshwater Science*, *39*(1), 126–136. https://doi.org/10.1086/707810

Pribyl, A. L., Mccutchan, J. H., Lewis, W. M., & Saunders III, J. F. (2005). Whole-system estimation of denitrification in a plains river: a comparison of two methods. *Biogeochemistry*, *73*(3), 439–455. https://doi.org/10.1007/s10533-004-0565-4

Qi, H., & Liu, Y. (2023). Nitrogen removal through denitrification in China's aquatic system. *Science of The Total Environment*, *891*, 164317. https://doi.org/10.1016/j.scitotenv.2023.164317

Quick, A. M., Reeder, W. J., Farrell, T. B., Tonina, D., Feris, K. P., & Benner, S. G. (2019). Nitrous oxide from streams and rivers: A review of primary biogeochemical pathways and environmental variables. *Earth-Science Reviews*, *191*, 224–262. https://doi.org/10.1016/j.earscirev.2019.02.021

Raymond, P. A., Zappa, C. J., Butman, D., Bott, T. L., Potter, J., Mulholland, P., Laursen, A. E., McDowell, W. H., & Newbold, D. (2012). Scaling the gas transfer velocity and hydraulic geometry in streams and small rivers. *Limnology and Oceanography: Fluids and Environments*, *2*(1), 41–53. https://doi.org/10.1215/21573689-1597669

Reisinger, A. J., Tank, J. L., Hoellein, T. J., & Hall, R. O. (2016). Sediment, water column, and open-channel denitrification in rivers measured using membrane-inlet mass spectrometry. *Journal of Geophysical Research: Biogeosciences*, *121*(5), 1258–1274. https://doi.org/10.1002/2015JG003261

Riddle, B., Fox, J., Ford, B., Husic, A., & Pollock, E. (2025). Fourteen-Year Fluvial Sediment Record Shows Non-Conservativeness of Organic Tracers: Recommendations for Sediment Fingerprinting. *Hydrological Processes*, *39*(1). https://doi.org/10.1002/hyp.70054

Soonmo, A. N., Gardner, W. S., & Kana, T. (2001). Simultaneous Measurement of Denitrification and Nitrogen Fixation Using Isotope Pairing with Membrane Inlet Mass Spectrometry Analysis. *Applied and Environmental Microbiology*, *67*(3), 1171–1178. https://doi.org/10.1128/AEM.67.3.1171-1178.2001

Speir, S. L., Tank, J. L., & Mahl, U. H. (2020). Quantifying denitrification following floodplain restoration via the two-stage ditch in an agricultural watershed. *Ecological Engineering*, *155*, 105945. https://doi.org/10.1016/j.ecoleng.2020.105945

Stanley, E. H., Casson, N. J., Christel, S. T., Crawford, J. T., Loken, L. C., & Oliver, S. K. (2016). The ecology of methane in streams and rivers: Patterns, controls, and global significance. In *Ecological Monographs* (Vol. 86, Issue 2, pp. 146–171). Ecological Society of America. https://doi.org/10.1890/15-1027

Strauss, E. A., & Lamberti, G. A. (2002). Effect of dissolved organic carbon quality on microbial decomposition and nitrification rates in stream sediments. *Freshwater Biology*, *47*(1), 65–74. https://doi.org/10.1046/j.1365-2427.2002.00776.x

Strauss, E. A., Mitchell, N. L., & Lamberti, G. A. (2002). Factors regulating nitrification in aquatic sediments: Effects of organic carbon, nitrogen availability, and pH. *Canadian Journal of Fisheries and Aquatic Sciences*, *59*(3), 554–563. https://doi.org/10.1139/f02-032

Taylor, P. G., & Townsend, A. R. (2010). Stoichiometric control of organic carbon-nitrate relationships from soils to the sea. *Nature*, *464*(7292), 1178–1181. https://doi.org/10.1038/nature08985

Upadhyay, P., Prajapati, S. K., & Kumar, A. (2023). Impacts of riverine pollution on greenhouse gas emissions: A comprehensive review. *Ecological Indicators*, *154*, 110649. https://doi.org/10.1016/j.ecolind.2023.110649

Verchot, L. V., Holmes, Z., Mulon, L., Groffman, P. M., & Lovett, G. M. (2001). Gross vs net rates of N mineralization and nitrification as indicators of functional differences between forest types. *Soil Biology and Biochemistry*, *33*(14), 1889–1901. https://doi.org/10.1016/S0038-0717(01)00095-5

Vincent, A. E. S., Tank, J. L., & Mahl, U. H. (2025). Seasonal patterns in sediment nitrification rates and their linkages to ammonium cycling in three agricultural streams. *Biogeochemistry*, *168*(1), 13. https://doi.org/10.1007/s10533-024-01196-2

Wachholz, A., Dehaspe, J., Ebeling, P., Kumar, R., Musolff, A., Saavedra, F., Winter, C., Yang, S., & Graeber, D. (2023). Stoichiometry on the edge—humans induce strong imbalances of reactive C:N:P ratios in streams. *Environmental Research Letters*, *18*(4). https://doi.org/10.1088/1748-9326/acc3b1

Wang, J., Wang, G., Zhang, S., Xin, Y., Jiang, C., Liu, S., He, X., McDowell, W. H., & Xia, X. (2022). Indirect nitrous oxide emission factors of fluvial networks can be predicted by

dissolved organic carbon and nitrate from local to global scales. *Global Change Biology*, *28*(24), 7270–7285. https://doi.org/10.1111/gcb.16458

Wang, S., Lan, B., Yu, L., Xiao, M., Jiang, L., Qin, Y., Jin, Y., Zhou, Y., Armanbek, G., Ma, J., Wang, M., Jetten, M. S. M., Tian, H., Zhu, G., & Zhu, Y. G. (2024). Ammonium-derived nitrous oxide is a global source in streams. *Nature Communications*, *15*(1). https://doi.org/10.1038/s41467-024-48343-9

Winkler, K., Fuchs, R., Rounsevell, M., & Herold, M. (2021). Global land use changes are four times greater than previously estimated. *Nature Communications*, *12*(1). https://doi.org/10.1038/s41467-021-22702-2

Wong, W. W., Pottage, J., Warry, F. Y., Reich, P., Roberts, K. L., Grace, M. R., & Cook, P. L. M. (2018). Stable isotopes of nitrate reveal different nitrogen processing mechanisms in streams across a land use gradient during wet and dry periods. *Biogeosciences*, *15*(13), 3953–3965. https://doi.org/10.5194/bg-15-3953-2018

Woodrow, R. L., White, S. A., Conrad, S. R., Wadnerkar, P. D., Rocher-Ros, G., Sanders, C. J., Holloway, C. J., & Santos, I. R. (2024). Enhanced stream greenhouse gas emissions at night and during flood events. *Limnology and Oceanography Letters*, *9*(3), 276–285. https://doi.org/10.1002/lol2.10374

Xia, L., Cao, J., Stüeken, E. E., Hu, W., & Zhi, D. (2022). Linkages between nitrogen cycling, nitrogen isotopes, and environmental properties in paleo-lake basins. *GSA Bulletin*, *134*(9–10), 2359–2372. https://doi.org/10.1130/B36290.1

Xu, W., Wang, G., Liu, S., Wang, J., McDowell, W. H., Huang, K., Raymond, P. A., Yang, Z., & Xia, X. (2024). Globally elevated greenhouse gas emissions from polluted urban rivers. *Nature Sustainability*. https://doi.org/10.1038/s41893-024-01358-y

Xu, X., Yang, Y., Zhou, Y., Ma, J., Li, J., Zhou, X., Zhao, X., Wu, F., & Song, K. (2025). Global patterns and drivers of coupling between anammox and denitrification processes across inland aquatic ecosystems. *Communications Earth and Environment*, *6*(1). https://doi.org/10.1038/s43247-024-01980-w

Yang, D., Wang, D., Chen, S., Ding, Y., Gao, Y., Tian, H., Cai, R., Yu, L., Deng, H., & Chen, Z. (2021). Denitrification in urban river sediment and the contribution to total nitrogen reduction. *Ecological Indicators*, *120*, 106960. https://doi.org/10.1016/j.ecolind.2020.106960

Graphical abstract

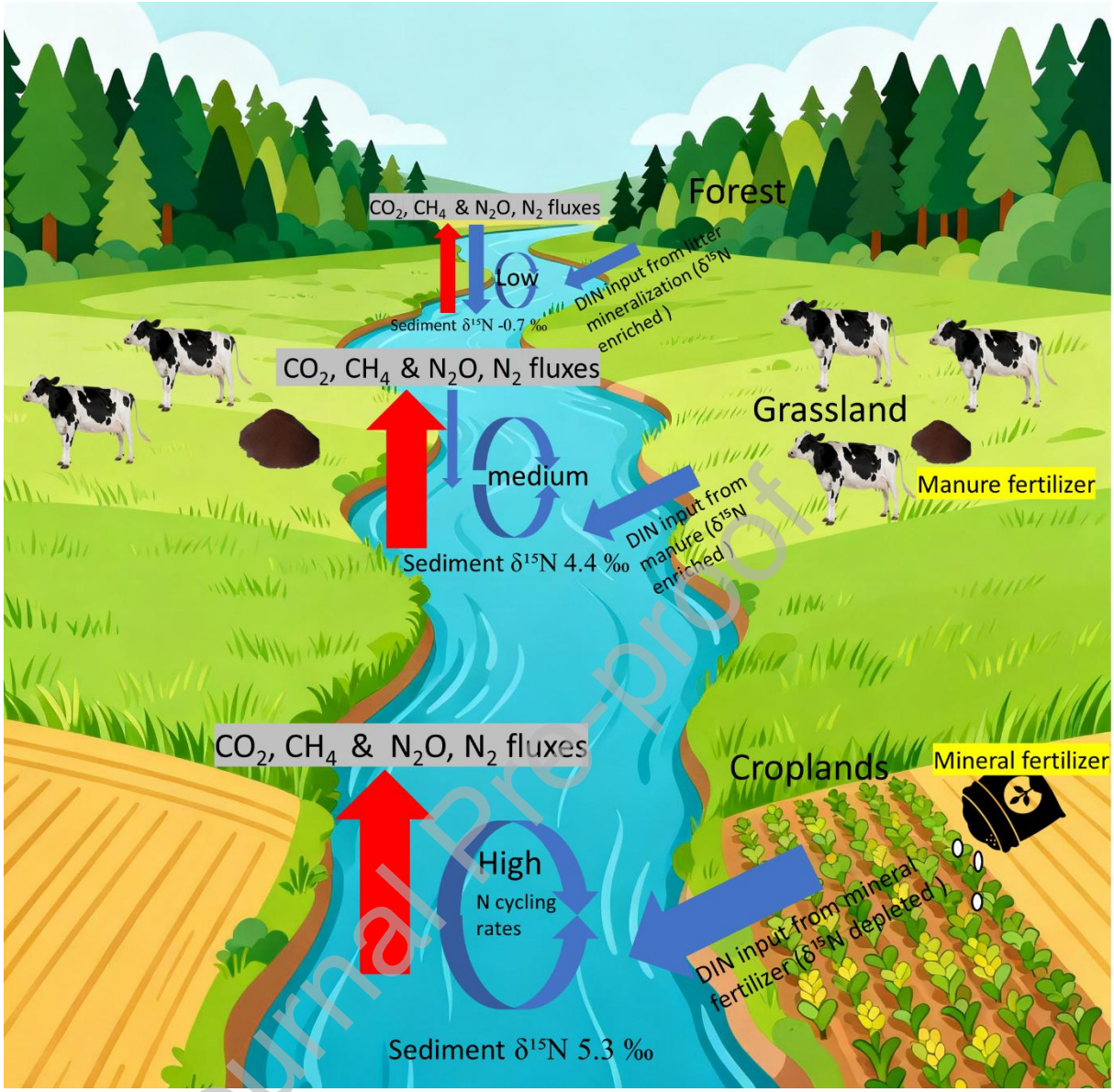

Declaration of interests

☒ The authors declare that they have no known competing financial interests or personal relationships that could have appeared to influence the work reported in this paper.